MAXIMUM ENTROPY QUADRATIC MODEL TO CHARACTERIZE CHEMICAL NON-EQUILIBRIUM IN RE-ENTRY FLOWS

BY

MAITREYEE SHARMA PRIYADARSHINI

THESIS

Submitted in partial fulfillment of the requirements
for the degree of Master of Science in Aerospace Engineering
in the Graduate College of the
University of Illinois at Urbana-Champaign, 2017

Urbana, Illinois

Adviser:

Assistant Professor Marco Panesi

ABSTRACT

This thesis presents the study of an advanced non-equilibrium model for state-specific chemical kinetics based on method of moments. The focus of this project is on the rovibrational chemical kinetics of the $N_2(^1\Sigma_g^+)$-$N(^4S_u)$ system. Internal excitation, dissociation, recombination and energy transfer reactions, which are important processes in aerothermodynamics, are studied. The kinetic and thermodynamic data is obtained from *ab-initio* calculations performed at NASA Ames Research Center. Previous analysis of the population distribution revealed that the population of the low lying energy levels of nitrogen molecules strongly deviates from a Boltzmann distribution, and the non-equilibrium distribution exhibits significant curvature. By invoking the maximum entropy principle subject to a series of constraints, the logarithm of distribution function is reconstructed using quadratic functions in the internal energy space of the molecular species. The results of the numerical simulations for an ideal chemical reactor show that the quadratic model captures the excitation and dissociation profiles accurately by using only three to seven groups thereby reducing the computational costs for non-equilibrium flow simulations significantly.

To my family and friends, for their love and support.

ACKNOWLEDGMENTS

Research is an emsemble of hardwork, collaboration and guidance. During the period of my masters, I was fortunate to have had the oppurtunity of working with wonderful minds who helped in the completion of this study. Firstly, I would like to acknowledge my advisor Prof. Marco Panesi for his guidance and support over the course of my masters research. I would like to express my gratitude to Dr. Yen Liu from NASA Ames Research Center who constantly guided me through the hurdles I faced in this project. My various discussions with Dr. Alessandro Munafo, Dr. Bruno Lopez and the entire NeqRad group aided in understanding various concepts and clarifying my queries. Finally, I express my heartful appreciation to my family for their constant support and encouragement.

TABLE OF CONTENTS

LIST OF FIGURES

CHAPTER 1

INTRODUCTION

Non-equilibrium flows occur during the entry or re-entry of a space vehicle into the planetary atmosphere. The re-entry occurs at hypersonic speeds giving rise to strong bow shocks in the forebody region as seen in figure 1.1. This heats up the gas to several thousand Kelvin which results in excitation of the internal energy modes of the molecules and change in composition of the gas mixture. These thermal and chemical process occur over a finite period of time known as the characteristic time for these process. This characteristic time is of the same order of magnitude as that of the flow characteristic time leading to flowfield with thermal and chemical non-equilibrium. These process have a prominent effect on the surface heating of the vehicle due radiation and convection. This nesseciates the use of well designed and appropriate thermal protection systems which facilitate the dissipation of heat from the surface of the vehicle by various methods like ablation, insulation etc.
Since the aerothermodynamic heating is very sensitive to the non-equilibrium processes in the flow, accurate characterization of non-equilibrium is vital. This study aims at modeling chemical non-equilibrium using first principles.

1.1 Objective and Overview

In the design of robust and effective thermal protection systems for spacecraft, it is vital that the heating on the surface of spacecraft moving at hypersonic speeds is predicted accurately. During entry of a space vehicle into the atmosphere of a planet, high temperatures reached in the shock layers change the state of the gas surrounding the spacecraft. The strong chemical non-equilibrium in the gas mixture causes changes in the energy distribution around the capsule thereby affecting the determination of heat loads on the

vehicular surface. Hence estimation of the heating depends strongly on the modeling and characterization of the non-equilibrium flow physics. Accurate modeling of non-equilibrium is also necessary for correct interpretation of data obtained through experiments in the shock tube, arc jet etc.

Currently, a tremendous effort is underway to study the microscopic interactions of the molecule-atom and molecule-molecule systems (Airforce/NASA). However, solving all these microscopic interactions from first principles is not practical since it is computationally very expensive. For example, the N_2-N system has 23 million reaction mechanisms possible. This number increases dramatically for molecule-molecule system due to the introduction of simultaneous excitation-dissociation as well as simultaneous excitation processes. Therefore, these limitations motivate the formulation of physics-based reduced order models in order to study non-equilibrium flows.

Therefore, the objective of the current study is to construct a new class of quantum-chemistry based models to enable truly predictive simulation of non-equilibrium chemistry phenomena, over a wide spectrum of flow conditions. Figure 1.2 give a pictorial representation of the objective of this project.

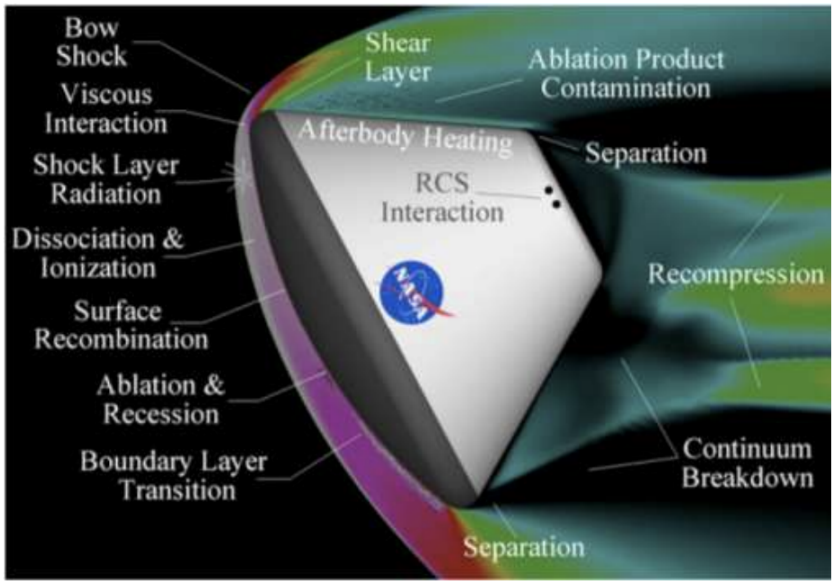

Figure 1.1: Flowfield around a hypersonic planetary re-entry vehicle
Source - Nasa Ames Research Center

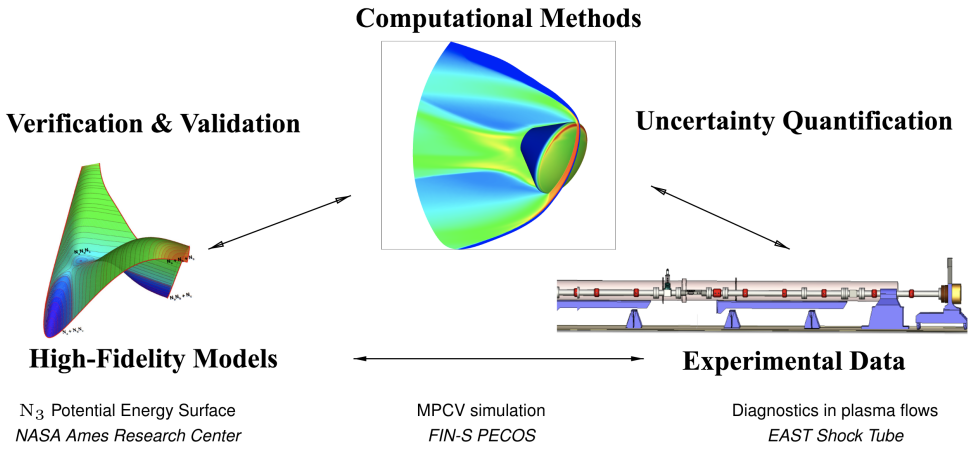

Figure 1.2: Objective: Work at the interface between computational chemistry, experimental measurements and CFD

The current work is dedicated to modeling the chemical kinetics of the $N_2(^1\Sigma_g^+)$-$N(^4S_u)$ system in a computationally efficient way. However, it should be kept in mind that the models developed in this thesis are applicable to any molecule system.

1.2 Literature Review

With the advancement in computational resources, detailed calculations of the reaction rates can be carried out [1, 2, 3, 4, 5]. Reaction rates govern the rate at which chemical reactions occur. They also determine the equilibrium constant and can be used to predict the equilibrium composition of a mixture. In these rate calculations, the first step is to obtain the Potential Energy Surface (PES); this is followed by calculation of the reaction rates by studying the collisional scattering using either quasi-classical trajectory (QCT)[6, 7, 8] or quantum approaches[9].

Departure of the population distribution function from the equilibrium Boltzmann distribution has a strong effect on the processes of dissociation [10, 11, 12, 13, 14, 15, 16, 17, 18, 19, 20, 21, 22, 23] and recombination [24, 25, 26, 27, 28, 29] which in turn affect the heating of the gas. The most accurate method to account for the non-equilibrium process is the state-to-state model, [30, 31, 32] which describes the evolution of the molecules in each energy state individually. Even though these methods are accurate,

they are computationally expensive due to the large number of energy states and possible reactions. Hence, it is impractical to include these methods in flow solvers to account for non-equilibrium dynamics [35, 36, 37, 38, 39]. Another approach to handle non-equilibrium flows is that of a multi-temperature model, where each internal energy mode follows an equilibrium distribution at a temperature corresponding to that energy mode [40, 41, 42]. However, this model is applicable only for flows where the deviation from equilibrium is very small.

The moment method was proposed to model translational non-equilibrium by Grad [43] and Levermore [44] in order to overcome the breakdown of the Chapman-Enskog expansion [45] in case of strong non-equilibrium conditions. An early attempt at modeling vibrational non-equilibrium was done by Landau and Teller [46]. This model is a linear relaxation model with various simplifying assumptions. Recently, Liu *et al.* [18, 19, 20] introduced a general methodology for modeling thermal and chemical non-equilibrium processes. In order to characterize the non-Boltzmann distribution, piece-wise representations of the distribution function were proposed. The quantum energy states of atoms and molecules are first subdivided into groups. A unified set of macroscopic equations for solving for both microscopic and macroscopic quantities are formulated by taking moments of the microscopic master equations. The microscopic solution is obtained by reconstruction based on the maximum entropy principle subject to the moment constraints, in which the logarithm of the distribution function in each energy group is expressed as a power series in internal energy. Macroscopic group rate coefficients are determined using the exact formulations but with the model distribution function. They are expressed as weighted sums of the corresponding microscopic rate coefficients, involving no tuning parameters or *ad hoc* fixes. Macroscopic modeling is considered as seeking the optimum reconstructed microscopic distribution function that provides converged and time accurate macroscopic quantities at all times. Through refinement of grouping and/or moment order, one can improve the accuracy of microscopic quantities and also check the convergence of macroscopic quantities. Since only moment equations are involved in the model, the number of differential equation to be solved is significantly reduced. The maximum entropy linear model was first published in 2010[18], there the macroscopic mass and internal energy equations for energy groups were obtained in a coupled manner from the

zeroth-order and first-order moments of the master equations. The formulation was later extended to high orders[19], and to general collisional and radiative processes[20]. Results of the linear model obtained in isothermal heat bath calculations have shown that accurate predictions of the macroscopic number density and internal energy are achievable by using only one to three energy groups, a total of 2 to 6 macroscopic equations[19, 20]. However, the linear model has also exhibited some deficiencies in predicting microscopic non-equilibrium populations if too few groups are used. [20]

In the multi-group models, the energy levels can be grouped together in various ways. Grouping is usually done based on a physical property of the levels where levels having close values for a property are grouped together. One such grouping technique which is also employed in this paper is the energy based grouping method. However, this method does not incorporate the kinetics of the system. An improved grouping strategy was proposed Sahai et. al. [47, 48]. This novel grouping strategy is based on the energy as well as the chemical kinetics of the system. The levels that are connected by 'fast' reactions tend to equilibrate with each other and hence are identified and grouped together. Two approaches are identified for grouping based on kinetics. One is the island algorithm which is derived from graph theory. The island algorithm finds points on a graph that are connected and lumps them together in an island. In the multi-group chemistry models, these islands are the groups of energy levels. Another technique developed for grouping energy levels is based on spectral clustering also from graph theory.

The current work presents a maximum entropy high order, modeling technique for non-equilibrium flows to address the deficiencies of the linear model. In this study, we use a piecewise quadratic representation for each group to describe the population distribution function. We focus on the rovibrational chemical kinetics of the $N_2(^1\Sigma_g^+)$-$N(^4S_u)$ system. While constructing the macroscopic governing equations we make no *ad hoc* assumptions regarding the internal energy modes of the molecule. The system can be generalized to involve other collisional and radiative processes if state-to-state rate coefficients become available. Note that the calculations to obtain **all** microscopic state-to-state rate coefficients would be very time consuming, and often impractical, for a collisional or radiative process. A new approach tailored for the model using Monte Carlo QCT that requires only a small fraction of the microscopic state-to-state coefficients to obtain converged macroscopic group

rate coefficients has been recently proposed by Macdonald *et al.* [49].

1.3 Thesis Organization

This thesis is organized in to 5 chapters. Chapter 1 is the introductory chapter. Chapter 2 describes the maximum entropy principle which is vital in formulation of the reduced order model. It also describes the exact system being studied which included the state to state kinetics of the $N_2(^1\Sigma_g^+)$-$N(^4S_u)$ system and the microscopic governing equations. This chapter lays the ground for building the reduced order model. The detailed derivation and formulation of the reduced order quadratic model is discussed in chapter 3. The chapter first discusses the method of moments applied in statistics. This method is used to form the macroscopic governing equations of the system. Various grouping strategies that can be used to club together internal states of the molecules are discussed. The exact macroscopic equations obtained from the microscopic equations are formulated with out any assumptions. Finally the chapter discusses the properties of the grouped chemical rates. The validation of this model against the state to state model is presented in chapter 4. This chapter shows the results of various numerical simulations run with different number of groups and different reconstruction operators including linear and quadratic reconstruction. The thesis is finally concluded in the last chapter.

CHAPTER 2

NON-EQUILIBRIUM FLOWS - PHYSICAL MODELING

There are 2 main aspects to the methodology developed. First is using the-maximum entropy principle in order to obtain a representation of the population distribution of the molecules in varies energy levels and second is the formulation of the macroscopic governing equations. This method involves the use of concepts of statistical mechanics and method of moments dicussed in the various sections of this chapter.

2.1 Maximum Entropy Principle

According to the postulates of thermodynamics, it is stated that in a system with no internal constraints, the extensive properties like internal energy, volume and number of particles, assume values that maximize the entropy of the system[50].

In the microcanonical ensemble of statistical thermodynamics, the Boltzmann equation gives a relation between the possible equiprobable microstates of a system and the entropy of the system. Maximum entropy is therefore related to W_{max}, which is the maximum number of microstates possible for a given macrostate. The Boltzmann's equation then describes the maximum entropy of a system in equilibrium as,

$$S_{max} = k_B \ln W_{max} \tag{2.1}$$

W_{max} can be described by either the Fermi-Dirac Statistics or the Bose-Einstein Statistics. However, in the dilute limit, when the number of states available is much larger than the number of particles both statistics converge to the Maxwell-Boltzmann Statistics. This assumption is particularly valid at the high temperatures in the flow field of a hypersonic re-entry vehicle.

Using the maximum entropy principle, the population distribution in the

internal energy space of the system can be described by the following Boltzmann distribution function,

$$n_i = n_{tot} \frac{g_i e^{\frac{\varepsilon_i}{k_B T}}}{Q} \tag{2.2}$$

Q represents the partition function and is given by the following equation,

$$Q = \sum g_i e^{\frac{\varepsilon_i}{k_B T}} \tag{2.3}$$

Here, g_i represents the degeneracy of the internal energy state 'i'. In the formulation of the new reduced order model, the entropy of each group is maximized and the distribution of the population in each group is given by a piecewise quadratic function.

2.1.1 Statistics

For a system of particles, the particles can be distributed in the various microstates (in this study, the internal energy states) based on two statistics:

- Fermi-Dirac Statistics
- Bose-Einstein Statistics

These two statistics depend on the nature of the particles being studied.

Fermi-Dirac Statistics

In this type of statistics, only one fermion(elementary particle) can occupy a given degenerate state. The number of ways in which fermions, n_i can occupy the energy levels is given by:

$$W_F = \prod_{i \epsilon I_g} \frac{g_i!}{(g_i - n_i)!} \tag{2.4}$$

By Sterling's Approximation, we get:

$$\ln W_F = \sum_{i \epsilon I_g} \left[n_i \ln \left(\frac{g_i - n_i}{n_i} \right) + g_i \ln \left(\frac{g_i}{g_i - n_i} \right) \right] \tag{2.5}$$

Bose-Einstein Statistics

In this type of statistics, there is no restriction on the number of bosons(elementary particles) that can occupy a given degenerate state. The number of ways in which the bosons, n_i can occupy the energy levels is given by:

$$W_B = \prod_{i \epsilon I_g} \frac{(n_i + g_i - 1)!}{(g_i - 1)! n_i!} \tag{2.6}$$

Assuming $g_i \gg 1$ and $n_i \gg 1$, by Sterling's Approximation, we get:

$$\ln W_B = \sum_{i \epsilon I_g} \left[n_i \ln \left(\frac{n_i + g_i}{n_i} \right) + g_i \ln \left(\frac{n_i + g_i}{g_j} \right) \right] \tag{2.7}$$

In the limiting case, we have $g_i \gg n_i$. In this dilute limit, both Fermi-Dirac and Bose-Einstein statistics converge to the Boltzmann Statistics, resulting in:

$$\ln W_B^F = \sum_{i \epsilon I_g} \left[n_i \ln \left(\frac{g_i \pm n_i}{n_i} \right) \mp g_i \ln \left(\frac{g_i \mp n_i}{g_i} \right) \right] \tag{2.8}$$

$$\ln W_B^F = \sum_{i \epsilon I_g} \left[n_i \ln(g_i \pm n_i) - n_i \ln(n_i) \mp g_i \ln(g_i \mp n_i) \pm g_i \ln(g_i) \right] \tag{2.9}$$

To find the value of W that maximizes the above equation, the derivative of the equation is computed.

$$d(\ln W_B^F) = \sum_{i \epsilon I_g} dn_i \left[\ln(g_i \pm n_i) \pm \frac{n_i}{g_i \pm n_i} - \ln(n_i) - 1 + \frac{g_i}{g_i \mp n_i} \right] \tag{2.10}$$

$$\begin{aligned} d(\ln W_B^F) &= \sum_{i \epsilon I_g} dn_i \left[\ln(g_i \pm n_i) - \ln(n_i) \right] \\ &= \sum_{i \epsilon I_g} dn_i \left[\ln \left(\frac{g_i \pm n_i}{n_i} \right) \right] \\ &= \sum_{i \epsilon I_g} dn_i \left[\ln \left(\frac{g_i}{n_i} \pm 1 \right) \right] \end{aligned}$$

Since $g_i \gg 1$, $n_i \gg 1$ and $g_i \gg n_i$, we get:

$$d(\ln W_B^F) = \sum_{i \epsilon I_g} dn_i \left[\ln \left(\frac{g_i}{n_i} \right) \right] \tag{2.11}$$

For W_{max},

$$d(\ln W_B^F) = \sum_{i \epsilon I_g} dn_i \left[\ln \left(\frac{g_i}{n_i} \right) \right] = 0 \tag{2.12}$$

2.2 State-to-State Kinetics

To study the application of the macroscopic model developed, chemical reactions occurring in the $N_2(^1\Sigma_g^+)$-$N(^4S_u)$ system are studied. By $N_2(^1\Sigma_g^+)$-$N(^4S_u)$ system it is meant that only reactions occurring due to the collisions of N_2 molecules and N atoms are considered, i.e. the collision partner in all reactions is the nitrogen atom, $N(^4S_u)$. For simplicity, no radiative processes are included in this paper. The state-to-state collision reactions considered include the rovibrational energy transfer interactions and dissociation-recombination reactions. The concentration of the chemical species is a function of time alone, i.e. the mixture is spatially homogeneous and the simulations are 0-D simulations. Electronic transitions and ionization reactions are ignored in this study. However, this is a generic model and can be applied for all kinetic (state-to-state collisional) and radiative processes.

The $N_2(^1\Sigma_g^+)$ molecule has 9390 rovibrational levels. The first 7421 levels are bound levels and the remaining are pre-dissociative or quasi bound. The state-to-state kinetics data for this system is obtained from the *ab initio* calculations done at NASA Ames Research Cente.[1, 3, 2, 4]. The rovibrational levels are sorted in the increasing order of their energy. There is no distinction between the rotation and vibration levels. They are treated in the same manner. The kinetics of this chemical system is discussed below.

The following represents the energy transfer reactions of the $N_2(^1\Sigma_g^+)$-$N(^4S_u)$ system:

$$N_2^i + N \Longleftrightarrow N_2^j + N$$

These reactions include momentum and energy transfer amongst the molecules and atoms. The index i and j in the reaction represent the rovibrational level

in the $N_2(^1\Sigma_g^+)$ molecule. There is no superscript on the collision partner since it is assumed that the collision partner does not undergo a change in its internal state during the reactions.

The other pair of reactions studied are the dissociation-recombination reactions. These can be represented as:

$$N_2^i + N \Longleftrightarrow N + N + N$$

These reactions also include mass transfer in addition to momentum and energy transfer.

2.3 Microscopic Governing Equations

There are over 40 x 10^6 rovibrational dissociation and energy transfer reactions possible in the $N_2(^1\Sigma_g^+)$-$N(^4S_u)$ system. The chemical master equation governing these reactions is discussed in this section.

Let $n_{N_2}^i$, g_i and ϵ_i denote the population, degeneracy and energy of rovibrational level i of the N_2 molecule. n_N denotes the number of nitrogen atoms. The excitation rate coefficients from level i to j are denoted by $k_{i,j}$ and the dissociation rate coefficients are denoted by k_i^d. These rate coefficients are calculated using an Arrhenius fit where the fit parameters are obtained from the calculations done at NASA Ames Research Center. The de-excitation rate coefficients $k_{j,i}$ and recombination rate coefficients k_i^r are computed using the relations of detailed balancing. The principle of detailed balancing relates the forward and backward rates of a chemical reaction by the equilibrium constant. The equilibrium constant can be expressed as a function of the degeneracy and energy value of the level. The following equations show the relationship between these various rate coefficients.

$$K_{eq}^{exc} = \frac{g_j}{g_i} \exp\left[\frac{-(\varepsilon_j - \varepsilon_i)}{k_B\ T}\right] \tag{2.13}$$

$$K_{eq}^{diss} = \frac{\left(g_N\ Q_N^{tr}\right)^2}{g_i\ Q_{N_2}^{tr}} \exp\left[\frac{-(2\varepsilon_N - \varepsilon_i)}{k_B\ T}\right] \tag{2.14}$$

$$Q^{tr} = \left(\frac{2\pi\ m\ k_B\ T}{h^2}\right)^{1.5} \tag{2.15}$$

K_{eq} is the notation used for the equilibrium constant either for the excitation-deexcitation reactions (exc) or dissociation-recombination reactions (diss). These equilibrium constants are used in the principle of detailed balancing to compute the reverse chemical rate coefficients. In the above equations, 'T' corresponds to the translation temperature of the system. The internal states equilibriate to this translation temperature. The symbol k_B represents the Boltzmann constant and 'h' is the Planck's constant. Q^{tr} is the translation partition function. In the translation partition function, 'm' is the mass of the single atom or molecule.

The microscopic deexcitation rate coefficient is given by the equation (2.16). Similarly, the recombination rates are given by equation (2.17)

$$k_{j,i} = \frac{k_{i,j}}{K_{eq}^{exc}} \tag{2.16}$$

$$k_i^r = \frac{k_i^d}{K_{eq}^{diss}} \tag{2.17}$$

The microscopic governing equation for the population density of the N_2 molecules is then written as,

$$\frac{dn_{N_2}^i}{dt} = \sum_{j \epsilon n} \left[-k_{i,j} n_{N_2}^i n_N + k_{j,i} n_{N_2}^j n_N \right] + \left[-k_i^d n_{N_2}^i n_N + k_i^r n_N^3 \right] \tag{2.18}$$

The first two terms in the master equation denote the change in the energy-state number density due to the excitation and de-excitation process. The last two terms in the rate equation denote the change in the individual state population density due to dissociation and recombination processes. The master equation, equation (2.18), has only a temporal derivative since it is assumed that the chemical reactions have no spatial dependence. The mole fractions have no spatial gradients.

This microscopic master equation is the pivotal point in the development of the advanced quadratic model characterizing chemical non-equilibrium which uses the method of moments.

CHAPTER 3

MAXIMUM ENTROPY QUADRATIC MODEL

Since it is impractical to solve the microscopic master equation (2.18), the method of moments is adopted to handle chemical and thermal non-equilibrium. Using this method, instead of solving the kinetics for each energy state of the molecule, particular macroscopic moments of the system are solved for. These macroscopic moments are used to reconstruct the state-to-state population distribution. The macroscopic moments used during reconstruction are such that they retain the physics of the system.

3.1 Method of Moments

Method of moments is widely used in statistics. In this method, the sampled moments are equated to theoretical moments of the random variable being studied. (The moments of a random variable are the estimated values of the powers of the random variable.) The basic idea in this method is forming as many moment equations as there are parameters to be solved and then solving for the parameters. These parameters are used to characterize the distribution function. For example, 'p' parameters are required to characterize the distribution of the random variable, then 'p' moments of the population distribution are computed which depend on the parameters, α_1,...,α_p [51]. Equations (3.1) represents these theoretical moments.

$$\begin{aligned} \mu_1 &\equiv E(X) = g_1(\alpha_1, \alpha_2, \ldots, \alpha_p), \\ \mu_2 &\equiv E(X^2) = g_2(\alpha_1, \alpha_2, \ldots, \alpha_p), \\ &\vdots \\ \mu_p &\equiv E(X^p) = g_p(\alpha_1, \alpha_2, \ldots, \alpha_p) \end{aligned} \tag{3.1}$$

To obtain the sampled moments, 'm' samples are drawn and the moments are then calculated as follows,

$$\hat{\mu}_j = \frac{1}{m} \sum_{i=1}^{m} w_i^j \tag{3.2}$$

where $\mathrm{w_i}$ is the $\mathrm{i^{th}}$ sample drawn and 'j' represents the power to which the sample value is raised. The $\mathrm{j^{th}}$ sampled moment is then given by $\hat{\mu_j}$. These depend on the estimated parameters denoted by $\hat{\alpha}_p$. Therefore, the following system of equations can be solved to obtain the parameters of the distribution function.

$$\begin{aligned} \hat{\mu}_1 &= g_1(\hat{\alpha}_1, \hat{\alpha}_2, \ldots, \hat{\alpha}_p), \\ \hat{\mu}_2 &= g_2(\hat{\alpha}_1, \hat{\alpha}_2, \ldots, \hat{\alpha}_p), \\ &\vdots \\ \hat{\mu}_p &= g_p(\hat{\alpha}_1, \hat{\alpha}_2, \ldots, \hat{\alpha}_p) \end{aligned} \tag{3.3}$$

One application of the method of moments is the estimation of the coefficients of a k^{th} order polynomial function used to approximate the probability distribution function of a random variable [52].

In this thesis, the method of moments along with polynomial reconstruction is utilized to formulate the reduced order model to characterize the non-equilibrium population distribution of molecules in a gas mixture. The formulation is discussed in the subsequent sections.

3.2 Grouping Strategies

One of the key aspects of the model reduction procedure is the grouping of internal levels into bins, the so-called level partitioning step. In order to solve a macroscopic system instead of treating individual energy states as a different species, it is required that energy states with certain similar properties are grouped together and solved for as one species. Various grouping strategies can be used [48, 47]. The effectiveness of these algorithms is evaluated by their ability to reproduce the exact state-to-state results for simple time-dependent simulations like an isothermal reactor. These algorithms range

from simple and efficient energy-based methods to very accurate methods based on the kinetics of the system. These advanced algorithms implement a modified island algorithm and a spectral clustering approach [48, 47]. A brief description of the grouping methods is given here.

- Uniform-energy method: This approach sub-divides the whole energy range of internal states into a set of uniform energy intervals, and all levels within each energy interval are then assigned to a given bin. To implement this method, all the internal energy states of the molecules are arranged in the ascending order and then the levels are divided in equal energy partitions where the number of partitions is equal to the number of groups desired.

- Closest-energy method: In this approach, instead of assuming an uniform sub-division of the entire energy range, the internal levels are grouped according to their energy spacing, the closest levels being grouped first. The underlying procedure is as follows. The internal levels are first arranged in the increasing order of their energy and the energy spacing between adjacent levels is calculated. The two closest levels are then grouped together, leading to one level less in the initial set of internal levels. The level grouping steps are repeated until the resulting number of levels matches the target number of groups. Note that the energy of a group corresponds to the average energy of all its sub-levels.

- Kinetic-based method: These methods use an adaptive grouping methodology based on both the magnitude of the transition rates and the energy of the internal levels. Levels that are close in energy and are related by fast transitions with respect to each other are grouped together. This is done since the rate determining process are always the slow processes and these are the process that lead to non-equilibrium. Therefore, grouping two levels that are very close in energy but interact via a transition rate that is low should not be grouped together. These kinetics based methods ensure this. Two approaches have been developed for adaptive grouping, one uses the a modified island algorithm and the other groups levels based on spectral clustering techniques.

The two energy-based approaches differ conceptually in the sense that the

former relies on the assumption of a uniform distribution of internal states within the electronic structure of the species, while the latter takes advantage of the actual energy spacing of the internal levels. However, for vibrational/rovibrational levels of small molecules, the uniform energy grouping is a valid approximation. Studying more complex geometry molecules like carbon dioxide it is imperative to use kinetic-based methods.

3.3 Exact Formulation - Macroscopic Moments Equation

The grouping strategy used in this study is uniform energy grouping, i.e. the entire energy space of the molecule is split into groups having equal energy intervals. This forces the states having energies close to each other to be lumped into the same group. The reconstruction operator used is a polynomial in energy for each internal state belonging to the group. This polynomial represents the logarithm of the population for each state belonging to that group, normalized by its degeneracy.

In order to arrive at the macroscopic moment equation, moments of the microscopic master equation (2.18) are taken. Various moments of equation (2.18) are then summed over all the levels belonging to each group. This reduces the number of ordinary differential equations from the order of rovibrational levels in the molecule to the order of the number of groups chosen to represent the energy space of the molecule. Following the approach of Liu *et al.* [19, 20], we obtain:

$$\sum_{i\epsilon I_g} \frac{dn^i_{N_2}}{dt} = \sum_{i\epsilon I_g}\sum_{h\epsilon I_n}\sum_{j\epsilon I_h}\left[-k_{i,j}n^i_{N_2}n_N \; + k_{j,i}n^j_{N_2}n_N\;\right] + \sum_{i\epsilon I_g}\left[-k^d_i n^i_{N_2}n_N + k^r_i n^3_N\right] \tag{3.4}$$

$$\begin{aligned}\sum_{i\epsilon I_g} \frac{de^i_{N_2}}{dt} &= \sum_{i\epsilon I_g}\sum_{h\epsilon I_n}\sum_{j\epsilon I_h}\left[-k_{i,j}\varepsilon_i n^i_{N_2}n_N \; + k_{j,i}\varepsilon_i n^j_{N_2}n_N\;\right] \\ &+ \sum_{i\epsilon I_g}\left[-k^d_i \varepsilon_i n^i_{N_2}n_N + k^r_i \varepsilon_i n^3_N\right]\end{aligned} \tag{3.5}$$

$$\sum_{i\epsilon I_g} \frac{df^i_{N_2}}{dt} = \sum_{i\epsilon I_g}\sum_{h\epsilon I_n}\sum_{j\epsilon I_h}\left[-k_{i,j}\varepsilon_i^2 n^i_{N_2} n_N + k_{j,i}\varepsilon_i^2 n^j_{N_2} n_N\right] + \sum_{i\epsilon I_g}\left[-k^d_i\varepsilon_i^2 n^i_{N_2} n_N + k^r_i\varepsilon_i^2 n^3_N\right] \quad (3.6)$$

The above equations are the exact macroscopic moment governing equations. No ad hoc assumptions are made in formulating these equations. The symbols used in the macroscopic moment equations are as follows. I_n denotes the total number of groups in the system. I_g and I_h refer to the set of energy levels belonging to the group g and group h, respectively. $n^g_{N_2}$, $e^g_{N_2}$ and $f^g_{N_2}$ represent the macroscopic moments of group g.

Further, the group rate coefficients are computed and equations (3.4)-(3.6) are rewritten using grouped macroscopic rate coefficients. $K_{g,h}$ denotes the group excitation rate coefficient for the excitation process occurring from group g to group h, and C^d_g represents the group dissociation rate from group g. Similarly, $K_{h,g}$ and C^r_g are the group de-excitation and recombination rate coefficients, respectively. The numerical index on these rate coefficients corresponds to the order of the moment for which the rate coefficient is being defined.

$$\frac{dn^g_{N_2}}{dt} = \sum_{h\epsilon I_n}\left[-{}^0K_{g,h} n^g_{N_2} n_N + {}^0K_{h,g} n^h_{N_2} n_N\right] - {}^0C^d_g n^g_{N_2} n_N + {}^0C^r_g n^3_N \quad (3.7)$$

$$\frac{de^g_{N_2}}{dt} = \sum_{h\epsilon I_n}\left[-{}^1K_{g,h} e^g_{N_2} n_N + {}^1K_{h,g} e^h_{N_2} n_N\right] - {}^1C^d_g e^g_{N_2} n_N + {}^1C^r_g n^3_N \quad (3.8)$$

$$\frac{df^g_{N_2}}{dt} = \sum_{h\epsilon I_n}\left[-{}^2K_{g,h} f^g_{N_2} n_N + {}^2K_{h,g} f^h_{N_2} n_N\right] - {}^2C^d_g f^g_{N_2} n_N + {}^2C^r_g n^3_N \quad (3.9)$$

The group rate coefficients are derived from the microscopic rate coefficients directly without making any simplifications or assumptions. The detailed derivations are attached in the appendix.

$$ {}^0K_{g,h} = \sum_{i \epsilon I_g} \sum_{j \epsilon I_h} \frac{k_{i,j} n^i_{N_2}}{n^g_{N_2}} \ , \ {}^1K_{g,h} = \sum_{i \epsilon I_g} \sum_{j \epsilon I_h} \frac{k_{i,j} \varepsilon_i n^i_{N_2}}{e^g_{N_2}} \ , \ {}^2K_{g,h} = \sum_{i \epsilon I_g} \sum_{j \epsilon I_h} \frac{k_{i,j} \varepsilon_i^2 n^i_{N_2}}{f^g_{N_2}} $$

The dissociation rates are similarly derived and can be represented by the relations given in equation (3.10).

$$ {}^0C^d_g = \sum_{i \epsilon I_g} \frac{k^d_i n^i_{N_2}}{n^g_{N_2}} \ , \qquad {}^1C^d_g = \sum_{i \epsilon I_g} \frac{k^d_i \varepsilon_i n^i_{N_2}}{e^g_{N_2}} \ , \qquad {}^2C^d_g = \sum_{i \epsilon I_g} \frac{k^d_i \varepsilon_i^2 n^i_{N_2}}{f^g_{N_2}} $$

The recombination rates are simply a summation of the individual microscopic recombination rate coefficients of the states belonging to a particular group since recombination rates do not depend on the internal energy state population distribution of the molecules. They depend only on the translation temperature of the system.

$$ {}^0C^r_g = \sum_{i \epsilon I_g} k^r_i, \qquad {}^1C^r_g = \sum_{i \epsilon I_g} k^r_i \varepsilon_i, \qquad {}^2C^r_g = \sum_{i \epsilon I_g} k^r_i \varepsilon_i^2 $$

3.4 Model Reduction

In this section, the reduced order model is developed using the maximum entropy principle and method of moments. The internal energy of each energy state of the molecule system is analogous to the random variable in the method of moments . The evolution of moments of the internal energy is studied numerically which are then used to reconstruct the probability distribution function of the population within each group. The procedure is discussed in detail in the following subsections.

3.4.1 Constraints

Since the entire energy spectrum can not be accurately reconstructed using a single group for all levels, the levels are partitioned into smaller groups and the method of moments is applied to each group. The moments of each group are subject to constraints based on the maximum entropy principle.

These constraints are conservation equations of the moments. The conservation of the first few moments have physically interpretable meanings. The zeroth moment conservation corresponds to conservation of mass. The first moment conservation corresponds to the conservation of the internal energy of the group. This imposition of the conservation of moments is analogous to equating the sampled moments to the theoretical moments in the method of moments. Since in the quadratic model a second order polynomial is used to approximate the distribution function, three moments are used.

$$\sum_{i \epsilon I_g} n_i = n_g \qquad \sum_{i \epsilon I_g} n_i \varepsilon_i = e_g \qquad \sum_{i \epsilon I_g} n_i \varepsilon_i^2 = f_g \tag{3.10}$$

Differentiating the equations illustrated above gives:

$$\sum_{i \epsilon I_g} dn_i = 0$$

$$\sum_{i \epsilon I_g} \varepsilon_i dn_i = 0$$

$$\sum_{i \epsilon I_g} \varepsilon_i^2 dn_i = 0$$

These are the constraints that the system is subjected to while finding the most probably macrostate (ie, one with the maximum number of microstates).

3.4.2 Equations obtained from Maximum Entropy Principle

Going back to chapter 2, we recall that the solution of equation (2.12) gives the distribution of microstates within the most probable macrostate of the system of particles. This equation however is subject to the constraints given in equation (3.10). Hence this is an over-constrained equation. Lagrange's multipliers (α_g, β_g and γ_g) are used to obtain the solution of the equation to find $\mathrm{W_{max}}$. Therefore, equation (2.12) is written as:

$$\sum_{i \epsilon I_g} \left[\ln \frac{g_i}{n_i} - \alpha_g - \beta_g \varepsilon_i - \gamma_g \varepsilon_i^2 \right] dn_i = 0 \tag{3.11}$$

The number of Lagrange multipliers used is equal to the order of the poly-

nomial used to reconstruct the population distribution function within the group. Infact, these Lagrange multipliers are indeed the coefficients of the polynomial used for population reconstruction with each group as shown below:

$$\ln \frac{g_i}{n_i} - \alpha_g - \beta_g \varepsilon_i - \gamma_g \varepsilon_i^2 = 0 \tag{3.12}$$

$$\ln \frac{g_i}{n_i} = \alpha_g + \beta_g \varepsilon_i + \gamma_g \varepsilon_i^2 \tag{3.13}$$

3.4.3 Solution for Lagrange multipliers

The Lagrange multipliers are unique for each group since the quadratic function used for reconstruction varies for each group depending on the group properties. Therefore, rewriting equation (3.13) as,

$$n_i = g_i e^{(-\alpha_g - \beta_g \varepsilon_i - \gamma_g \varepsilon_i^2)} \tag{3.14}$$

and summing over all the levels belonging to a particular group, we get:

$$\sum_{i \epsilon I_g} n_i = \sum_{i \epsilon I_g} g_i e^{(-\alpha_g - \beta_g \varepsilon_i - \gamma_g \varepsilon_i^2)} \tag{3.15}$$

$$n_g = \sum_{i \epsilon I_g} g_i e^{(-\alpha_g - \beta_g \varepsilon_i - \gamma_g \varepsilon_i^2)} \tag{3.16}$$

The constant term in the quadratic representation of the energy-state population distribution, α_g, is related to the number of moles in the group and the zeroth partition function by the following relation,

$$e^{(-\alpha_g)} = \frac{n_g}{Q_g} \tag{3.17}$$

where, Q_g is referred to as the group partition function and depends on the slope and curvature term of the quadratic function. The first coefficient, α_g, can be viewed as a normalizing constant.

$$Q_g = \sum_{i \epsilon I_g} g_i e^{(-\beta_g \varepsilon_i - \gamma_g \varepsilon_i^2)}$$

Similarly, the higher moments can be written as:

$$e_g = \sum_{i \epsilon I_g} g_i \varepsilon_i e^{(-\alpha_g - \beta_g \varepsilon_i - \gamma_g \varepsilon_i^2)} \tag{3.18}$$

Substituting for $e^{(-\alpha_g)}$,

$$\frac{e_g}{n_g} = \frac{\sum\limits_{i \epsilon I_g} g_i \varepsilon_i e^{(-\beta_g \varepsilon_i - \gamma_g \varepsilon_i^2)}}{Q_g} \tag{3.19}$$

$$f_g = \sum_{i \epsilon I_g} g_i \varepsilon_i^2 e^{(-\alpha_g - \beta_g \varepsilon_i - \gamma_g \varepsilon_i^2)} \tag{3.20}$$

$$\frac{f_g}{n_g} = \frac{\sum\limits_{i \epsilon I_g} g_i \varepsilon_i^2 e^{(-\beta_g \varepsilon_i - \gamma_g \varepsilon_i^2)}}{Q_g} \tag{3.21}$$

Substituting for W_{max} in (2.1) we get,

$$\begin{aligned} S &= k \left[\sum_{i \epsilon I_g} n_i \left(\ln \frac{g_i}{n_i} \right) + \sum_{i \epsilon I_g} n_i \right] \\ &= k \left[\sum_{i \epsilon I_g} n_i \left(\alpha_g + \beta_g \varepsilon_i + \gamma_g \varepsilon_i^2 \right) + n \right] \\ &= k \left(\alpha_g n_g + \beta_g e_g + \gamma_g f_g \right) + k n_g \\ S &= \left(k \alpha_g n_g + k \beta_g e_g + k \gamma_g f_g \right) + k n_g \end{aligned} \tag{3.22}$$

Differentiating S with respect to e_g we obtain,

$$\frac{\partial S}{\partial e_g} = \left(k n_g \frac{\partial \alpha_g}{\partial e_g} + k \beta_g + k e_g \frac{\partial \beta_g}{\partial e_g} + k f_g \frac{\partial \gamma_g}{\partial e_g} + k \gamma_g \frac{\partial f_g}{\partial e_g} \right) \tag{3.23}$$

The Gibbs relation gives an expression for the derivative of the entropy with respect to energy of the system at equilibrium. The Gibbs relation is shown in equation (3.24). T_g is the group internal temperature at equilibrium.

$$\frac{\partial S}{\partial e_g} = \frac{1}{T_g} \tag{3.24}$$

Since 'f', the second moment is independent of the group internal energy,

'e', $\frac{\partial f_g}{\partial e_g} = 0$. Therefore, equating (3.23) and equation (3.24), we get:

$$\left(kn_g\frac{\partial \alpha_g}{\partial e_g} + ke_g\frac{\partial \beta_g}{\partial e_g} + kf_g\frac{\partial \gamma_g}{\partial e_g}\right) + k\beta_g = \frac{1}{T_g} \tag{3.25}$$

From equation (3.17),

$$\alpha_g = \ln\left[\sum_{i\epsilon I_g} g_i e^{-\beta_g\varepsilon_i - \gamma_g\varepsilon_i^2}\right] - \ln n_g \tag{3.26}$$

$$\frac{\partial \alpha_g}{\partial e_g} = \frac{\partial \alpha_g}{\partial \beta_g}\frac{\partial \beta_g}{\partial e_g} + \frac{\partial \alpha_g}{\partial \gamma_g}\frac{\partial \gamma_g}{\partial e_g} \tag{3.27}$$

$$\begin{aligned}
\frac{\partial \alpha_g}{\partial e_g} &= \frac{\partial \beta_g}{\partial e_g}\frac{1}{\sum\limits_{i\epsilon I_g} g_i e^{(-\beta_g\varepsilon_i-\gamma_g\varepsilon_i^2)}}\sum_{i\epsilon I_g}\left[g_i e^{(-\beta_g\varepsilon_i-\gamma_g\varepsilon_i^2)}\left(-\varepsilon_i - \frac{\partial \gamma_g}{\partial \beta_g}\varepsilon_i^2\right)\right] \\
&+ \frac{\partial \gamma_g}{\partial e_g}\frac{1}{\sum\limits_{i\epsilon I_g} g_i e^{(-\beta_g\varepsilon_i-\gamma_g\varepsilon_i^2)}}\sum_{i\epsilon I_g}\left[g_i e^{(-\beta_g\varepsilon_i-\gamma_g\varepsilon_i^2)}\left(-\frac{\partial \beta_g}{\partial \gamma_g}\varepsilon_i - \varepsilon_i^2\right)\right] \\
\frac{\partial \alpha_g}{\partial e_g} &= \frac{\partial \beta_g}{\partial e_g}\frac{\sum\limits_{i\epsilon I_g}\left(g_i\varepsilon_i e^{(-\beta_g\varepsilon_i-\gamma_g\varepsilon_i^2)}\right) - \frac{\partial \gamma_g}{\partial \beta_g}\sum\limits_{i\epsilon I_g}\left(g_i\varepsilon_i^2 e^{(-\beta_g\varepsilon_i^2-\gamma_g\varepsilon_i^2)}\right)}{Q_g} \\
&+ \frac{\partial \gamma_g}{\partial e_g}\frac{\frac{\partial \beta_g}{\partial \gamma_g}\sum\limits_{i\epsilon I_g}\left(g_i\varepsilon_i e^{(-\beta_g\varepsilon_i-\gamma_g\varepsilon_i^2)}\right) - \sum\limits_{i\epsilon I_g}\left(g_i\varepsilon_i^2 e^{(-\beta_g\varepsilon_i^2-\gamma_g\varepsilon_i^2)}\right)}{Q_g}
\end{aligned} \tag{3.28}$$

We know that,

$$\frac{\partial \gamma_g}{\partial \beta_g} = 0 \tag{3.29}$$

$$\frac{\partial \beta_g}{\partial \gamma_g} = 0$$

because β_g and γ_g are independent variables.

Substituting from equations (3.19) and (3.21),

$$\frac{\partial \alpha_g}{\partial e_g} = -\frac{e_g}{n_g}\frac{\partial \beta_g}{\partial e_g} - \frac{f_g}{n_g}\frac{\partial \gamma_g}{\partial e_g} \tag{3.30}$$

Putting equation 3.30 in equation (3.25)

$$k\beta_g + \left[-ke_g\frac{\partial\beta_g}{\partial e_g} - kf_g\frac{\partial\gamma_g}{\partial e_g} + ke_g\frac{\partial\beta_g}{\partial e_g} + kf_g\frac{\partial\gamma_g}{\partial e_g}\right] = \frac{1}{T_g} \tag{3.31}$$

Therefore, at equilibrium we get,

$$\beta_g = \frac{1}{kT_g} \tag{3.32}$$

This is consistent with the physical relation that should be arrived at equilibrium since at equilibrium, the distribution relaxes to a Boltzmann distribution which is a straight line with slope inversely proportional to the temperature of the system.

3.4.4 Multi-Group Maximum Entropy Quadratic Formulation

Figure 3.1 shows a pictorial representation of the model reduction approach developed. Initially, the internal states of the molecule (blue dots) are grouped together based on some grouping strategy, uniform grouping in this study. This is followed by treating all the levels within a group as a single entity (red dot) and solving for the moments of this single grouped level. Once the moments of each group are estimated the population is then reconstructed using a piece-wise polynomial(blue line) to obtain the non-equilibrium distribution. It should be noted that the population distribution within each group is not known a priori. The blue dots are shown just to briefly explain the grouping process.

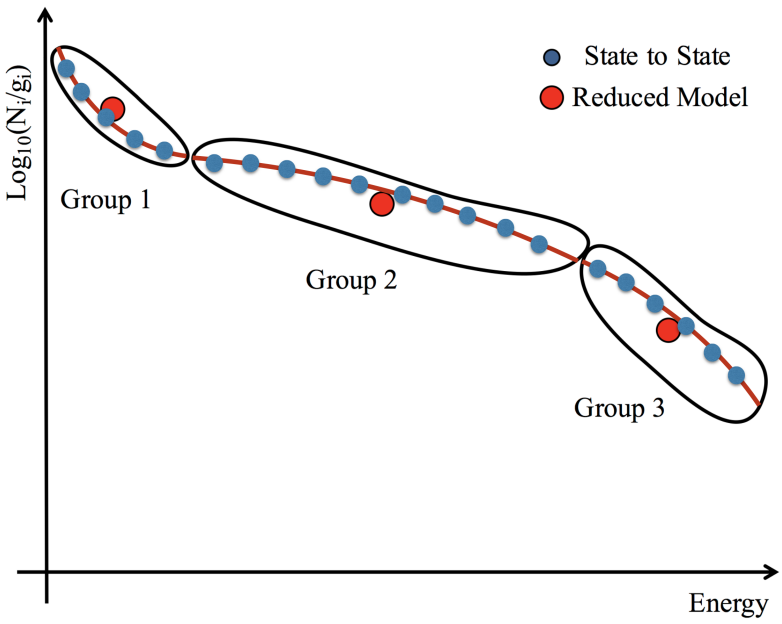

Figure 3.1: Population reconstruction from macroscopic moments

This section is used to describe the reconstruction operator used in the maximum entropy quadratic model. A quadratic function in energy is used to describe the energy state population distribution function within each group. The population distribution within each group is given by[18, 19, 20]

$$\ln \frac{g_i}{n_i} = \alpha_g + \beta_g \varepsilon_i + \gamma_g \varepsilon_i^2, \qquad i \in I_g \tag{3.33}$$

The parameters used in describing the microscopic population distribution within each group are functions of the macroscopic moments of that particular group, equation (3.34).

$$\alpha_g = \alpha_g(n_g, e_g, f_g), \quad \beta_g = \beta_g(n_g, e_g, f_g), \quad \gamma_g = \gamma_g(n_g, e_g, f_g) \tag{3.34}$$

This system of equations is used to describe the thermodynamic state of the system of molecules.

When the system reaches equilibrium, using the concept of Lagrange Multipliers and Maximum Entropy Principle, the value of β_g of each group is derived earlier to be related to the Boltzmann constant(k_B) and the final equilibrium temperature of the system.

$$\beta_g = \frac{1}{k_B T} \tag{3.35}$$

At equilibrium, the temperatures of all the groups are equal to each other and equal to the translational temperature of the system. The derivation of the slope(β) and curvature(γ) parameters also suggests that at equilibrium the value of γ_g for all groups tends to zero. This outcome is physically significant since, at equilibrium, the population distribution of the molecules attains a Boltzmann distribution which is a straight line in the log scale which implies that the curvature terms should go to zero.

Substituting equations (3.33) and (3.17) in equations (3.10) and (3.10) the group rate coefficients are obtained. Note that we do not make any *ad hoc* assumptions in calculating these rate coefficients and hence the physics of the system is retained to a large extent in this model satisfying the objective of this study.

3.5 Group Properties

The macroscopic group rate coefficients for the mth moment are given by equations (3.36) and (3.37). ${}^{m}Q_g$ in these expressions denotes the mth moment group partition function for the group g. The partition function is a normalization parameter and can be described as a weighted sum of probabilities of finding a molecule in a particular group. Equation (3.38) gives the form of the partition function. An exhaustive description of the grouped properties can be found in the paper by Liu *et al* [20].

$${}^{m}K_{g,h} = \frac{1}{{}^{m}Q_g} \sum_{i \epsilon I_g} \sum_{j \epsilon I_h} k_{i,j} \varepsilon_i^m g_i e^{-\beta_g \varepsilon_i - \gamma_g \varepsilon_i^2} \tag{3.36}$$

$${}^{m}C_g^d = \frac{1}{{}^{m}Q_g} \sum_{i \epsilon I_g} k_i^d \varepsilon_i^m g_i e^{-\beta_g \varepsilon_i - \gamma_g \varepsilon_i^2} \tag{3.37}$$

$${}^{m}Q_g = \sum_{i \epsilon I_g} g_i \varepsilon_i^m e^{-\beta_g \varepsilon_i - \gamma_g \varepsilon_i^2} \tag{3.38}$$

In the quadratic model, $m = 0, 1, 2$ corresponds to the first three moments of the microscopic population distribution function. The value of m depends on the degree of the polynomial used to describe the population distribution.

On solving for the macroscopic moments using equations (3.7) - (3.9), the moment values are obtained at every instant of time. Using this result, we solve for the quadratic parameters $(\alpha_g, \beta_g, \gamma_g)$ at every time step and then reconstruct the energy state population distribution.

3.5.1 Computation of α_g, β_g and γ_g

In order to first formulate an algorithm to determine the values of α_g, β_g and γ_g, a test case is created. This is represented in the figure below. Figure 3.2

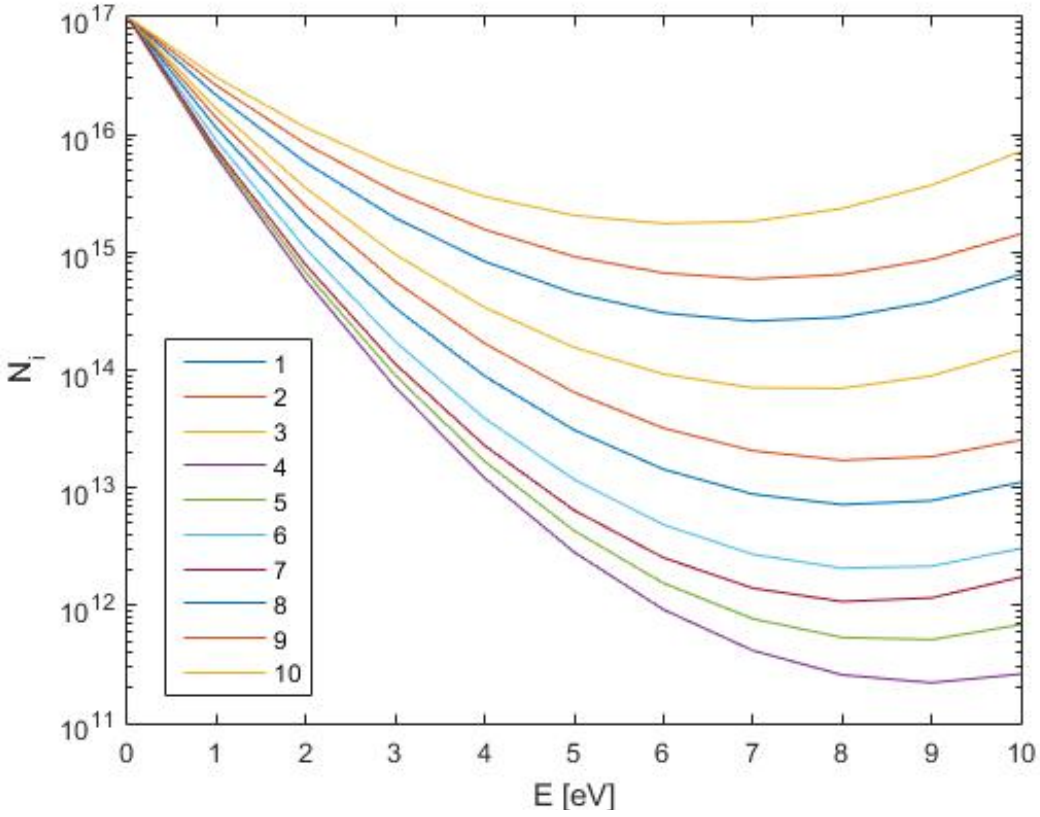

Figure 3.2: Population distribution in various energy levels in Non-equilibrium flow

represents the population distribution within various energy levels in a non-equilibrium flow. The different lines correspond to different values of α_g, β_g and γ_g in equation (3.33). The degeneracy of each energy level is taken as unity, $g_i = 1$. It is noticed that γ_g has very high values of the order of 10^{36}

and hence to normalize the value, γ_g is represented by the following equation:

$$\gamma_g = \frac{1}{(kT_g)^2} \tag{3.39}$$

where T_g is a temperature and k is the Boltzmann constant.
The algorithm implemented is as follows:

- In order to estimate the values of β_g and γ_g, Newton Raphson's method to solve nonlinear equations is used. The equations solved using Newton Raphson are:

$$F_2(\alpha_g, \beta_g, \gamma_g) = \sum_{i \epsilon I_g} \left[g_i \varepsilon_i e^{(-\alpha_g - \beta_g \varepsilon_i - \gamma_g \varepsilon_i^2)} \right] - e_g \tag{3.40}$$

$$F_3(\alpha_g, \beta_g, \gamma_g) = \sum_{i \epsilon I_g} \left[g_i \varepsilon_i^2 e^{(-\alpha_g - \beta_g \varepsilon_i - \gamma_g \varepsilon_i^2)} \right] - f_g \tag{3.41}$$

- n_g,e_g and f_g are obtained from figure 3.2. In this test run only one group is considered.

- The jacobian of this system of equations is a 3×3 matrix and is as follows:

$$J = \begin{bmatrix} \frac{\partial F_2}{\partial \beta_g} & \frac{\partial F_2}{\partial \gamma_g} \\ \\ \frac{\partial F_3}{\partial \beta_g} & \frac{\partial F_3}{\partial \gamma_g} \end{bmatrix} \tag{3.42}$$

- The Newton Raphson formulation of the problem is shown below:

$$\begin{Bmatrix} \Delta\beta_g \\ \Delta\gamma_g \end{Bmatrix} = -J^{-1} \begin{Bmatrix} F_2(\alpha_g, \beta_g, \gamma_g) \\ F_3(\alpha_g, \beta_g, \gamma_g) \end{Bmatrix} \tag{3.43}$$

$$\begin{Bmatrix} \beta_{i+1} \\ \gamma_{i+1} \end{Bmatrix} = \begin{Bmatrix} \beta_i \\ \gamma_i \end{Bmatrix} + \begin{Bmatrix} \Delta\beta_g \\ \Delta\gamma_g \end{Bmatrix} \tag{3.44}$$

  where i is just a counter.

The tables below shows the actual values and the estimated values.

Table 3.1: Comparison of Actual values with Estimated values

Plot No.	Variable	Actual Value	Estimated Value
1	α_g	-39.14394658	-39.14394660
	β_g	1.44927536e+19	1.44864596e+19
	γ_g	-5.50e+36	-5.50001832e+36
2	α_g	-39.14394658	-39.14394658
	β_g	1.31695046e+19	1.31695048e+19
	γ_g	-5.00e+36	-5.00000073e+36
3	α_g	-39.14394658	-39.14394658
	β_g	1.20720459e+19	1.20720459e+19
	γ_g	-5.00e+36	-5.00000007e+36
4	α_g	-39.14394658	-39.14394658
	β_g	1.810806895e+19	1.81080697e+19
	γ_g	-6.30e+36	-6.30000437e+36
5	α_g	-39.14394658	-39.14394667
	β_g	1.76664087e+19	1.76664682e+19
	γ_g	-6.40e+36	-6.40030933e+36
6	α_g	-39.14394658	-39.14394658
	β_g	1.60960612e+19	1.60960615e+19
	γ_g	-6.00e+36	-6.00000110e+36
7	α_g	-39.14394658	-39.14394658
	β_g	1.72457799e+19	1.72457819e+19
	γ_g	-6.50e+36	-6.50000969e+36
8	α_g	-39.14394658	-39.14394658
	β_g	1.03474679e+19	1.03474681e+19
	γ_g	-4.50e+36	-4.50000045e+36
9	α_g	-39.14394658	-39.14394658
	β_g	9.05403447e+18	9.05403449e+18
	γ_g	-4.00e+36	-4.00000003e+36
10	α_g	-39.14394658	-39.14394658
	β_g	8.04803064e+18	8.04803064e+18
	γ_g	-4.00e+36	-4.00000000e+36

CHAPTER 4

RESULTS: APPLICATION TO HEAT BATH

Chemical non-equilibrium processes are studied by carrying out simulations of an isothermal reactor. The temperature of the reactor is initially 2,000 K. A mixture of 95% N_2 and 5% N is introduced in the reactor. The temperature of the reactor is increased to 20,000 K. Translation modes of the N_2-N system equilibrate to the temperature of 20,000 K instantly. The strong chemical non-equilibrium state within the ro-vibrational levels of the N_2-N system is studied to validate the proposed model.

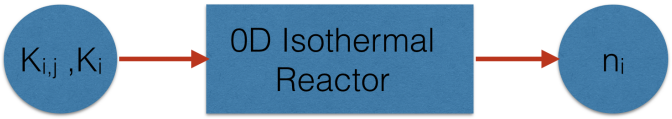

Figure 4.1: 0-D Isothermal Reactor

0-D Isothermal Reactor
Initial Temperature : 2,000 K
Final Temperature : 20,000 K
N_2 : 95% N : 5%
Number of levels : 7421
ODE Solver : CVODE

4.1 Nitrogen System

Validation of the maximum entropy quadratic model is done by comparison of the solutions obtained by simulating the full state-to-state model discussed in section 2.3 and the solutions of the macroscopic governing equations (3.7)-(3.9) discussed in section 3.3.

These equations represent a set of stiff non-linear ordinary differential equations (ODE). In order to solve this system of ODEs, Backward Euler Scheme is employed. For the simulations carried out in this study, CVODE is chosen as the ODE solver, which is a part of the package SUNDIALS [53]. In order to solve the non-linear system of equations as seen in equation (3.34), we adopt the non-linear equation solver, KINSOL, also from the SUNDIALS package. CVODE and KINSOL use a LAPACK based direct solver, where LAPACK is run in parallel using OpenMP. The microscopic rate coefficients are also calculated in parallel using OpenMP.

The analytical jacobian is derived and used in newton iterations. This facilitates in reducing the computation time of the simulation drastically by avoiding the number of computations required to find the jacobian numerically.

4.1.1 Comparison of State Population Distribution

Accurate representation of the microscopic state population distribution is necessary to study the collisional and radiative processes and non-equilibrium behavior of a system of molecular species. The quadratic and linear max-entropy models are used to study the N_2-N system for varying number of bins. The reactions accounted for in the simulations comprise of the energy transfer reactions and dissociation-recombination reactions. A comparison of the full state population distribution is done for the quadratic model at various simulation times. Two quadratic cases are studied: 2 bins and 3 bins. Energy based binning is employed for both linear and quadratic bins.

Equation (2.18) is solved to obtained the temporal evolution of the full state-to-state population distribution. The microscopic reaction rates are obtained from the *ab-initio* calculations carried out at NASA Ames Research Center [3, 4, 5]. Macroscopic group quantities are obtained by solving equation (3.7) - (3.9) from which the population distribution is reconstructed using equation (3.33).

In figure 4.2, it is observed that the 1^{st} linear bin deviates from the full state solution significantly. Comparing this to the 1^{st} quadratic bin, it can be seen that the quadratic model provides a better representation of the state-to-state population distribution. The ability of the quadratic model to

account for the curvature in the distribution function helps in obtaining a better depiction of the kinetics of the system of molecules.

During initial excitation, the results obtained by using 2 quadratic groups and the results from the linear reconstruction are similar for the first group. Both models provide an inaccurate representation of the population distribution. The representation by the quadratic model is inaccurate only during the first few time steps whereas the linear model provides a poor representation throughout the simulation.

To overcome the inability to accurately depict the population distribution in the initial time steps using just 2 bins, a simulation with 3 quadratic groups is run. Figure 4.3 shows a comparison of the three models. Reconstruction using 3 quadratic groups show promising representation of the non-equilibrium behavior of the system at all times. Towards the end of the simulation when the energy transfer reactions are no more prominent, the curvature of the distribution functions tends to infinity. This means that the distribution approaches the Boltzmann distribution at 20,000 K. The quadratic parameter γ which corresponds to the curvature of the function tends to zero as we approach equilibrium which is a physically meaningful result.

The distribution function temporally evolves from a Boltzmann distribution at 2,000 K following intermediate non-Boltzmann distributions to a Boltzmann distribution at 20,000 K. The slope of the initial distribution is higher than the final distribution since the slope of the plot is inversely proportional to the temperature of the system: higher the temperature lower the slope. When the simulation starts, higher energy states start equilibrating and adapting to the final temperature faster. The lower energy states are frozen at the beginning of the simulation. At $t = 1.58489E - 13s$, the higher levels start approaching the Bolztmann distribution at the final translation temperature while the lower levels are in strong non-equilibrium. As we march forward in the simulation time, it can be seen that the non-Bolztmann distributions are correctly reconstructed using the quadratic model at every time instant. The moment values and hence, the slope as well as the curvature values in the quadratic formulation change continuously such that the state population distribution is reconstructed accurately. This can be seen in Figure 4.2a and 4.2b.

The dissociation limit of N_2 molecule is equal to 9.753 eV. Hence, molecules

which have the energy equal to the dissociation limit dissociate instantaneously. This causes the population to plummet at the dissociation limit which is seen in the plots of the population distribution function.

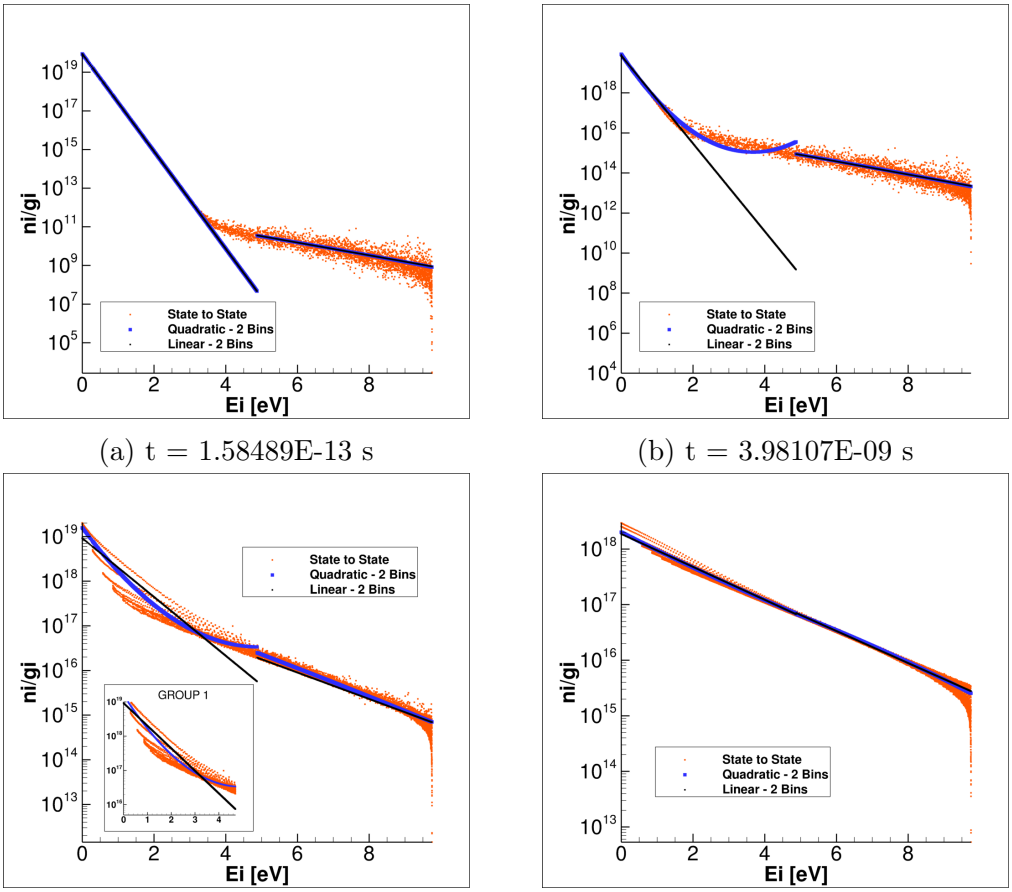

(a) t = 1.58489E-13 s

(b) t = 3.98107E-09 s

(c) t = 1.00000E-07 s

(d) t = 2.51189E-07 s

Figure 4.2: Comparison of the State Population distribution obtained using the State-to-State model and the Quadratic model

Another interesting feature is observed in the full state population distribution at around 0.1 μs. In the lower energy states, distinct strands separate out. As we move higher in the energy space, the strands dissolve into an undefined geometrical form. It is noticed that the energy states connected by these strands have the same vibrational quantum number. This implies that the rotational states belonging to the same vibration energy state tend to equilibrate faster which gives rise to these strands. The quadratic model using 2 or 3 bins is able to provide an averaged representation of the curvature of these strands. However, it is not able to mimic the strands individually

because in the binning strategy employed in this study, the kinetics of the chemical system is not considered.

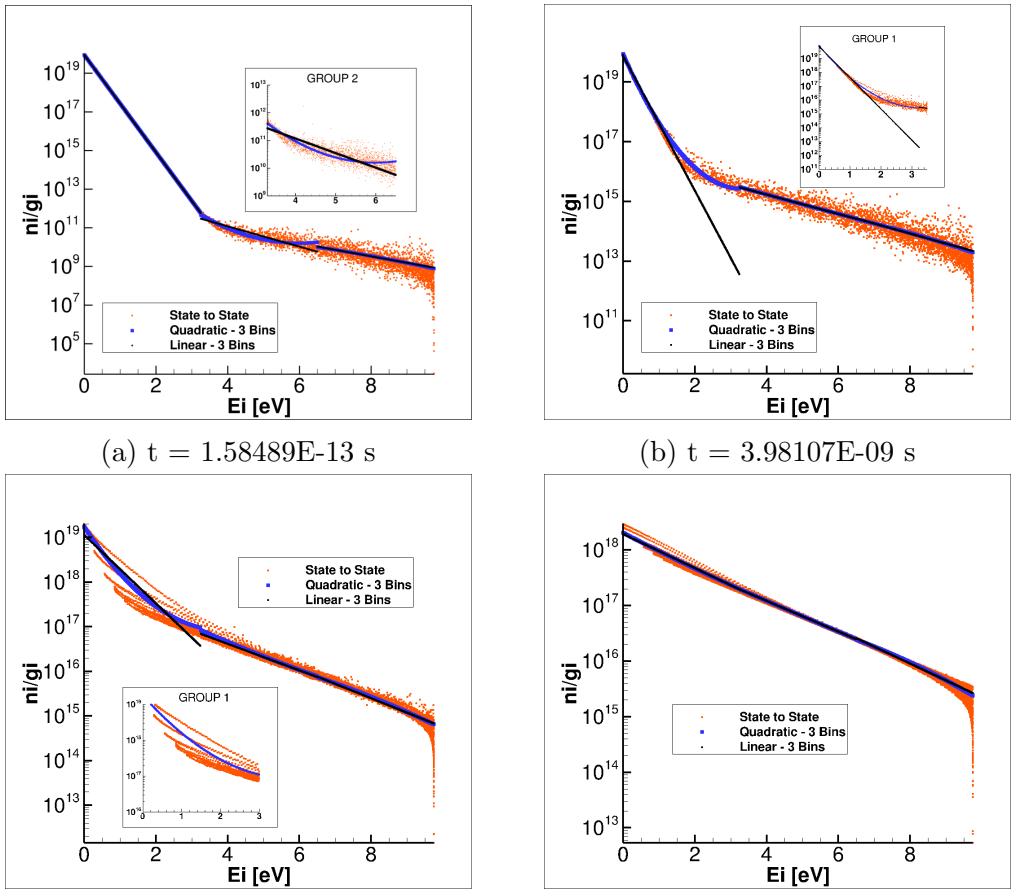

(a) t = 1.58489E-13 s

(b) t = 3.98107E-09 s

(c) t = 1.00000E-07 s

(d) t = 2.51189E-07 s

Figure 4.3: Comparison of the State Population distribution obtained using the State-to-State model and the Quadratic model

4.1.2 Comparison of Group Properties

Group properties are vital in the determination of the quadratic parameters which are used to reconstruct the state-to-state population distribution function. Equation (3.34) shows that the quadratic parameters are functions of the macroscopic group parameters. However, these functions are non-linear and can not be inverted to calculate the quadratic parameters directly. Therefore, it is imperative to use an iterative root-finding algorithm. The package KINSOL from SUNDIALS is used with inexact Newton iterations to obtain the values of the quadratic parameters from this system of

coupled non-linear equations.

Group quantities are obtained by numerically integrating the equations (3.7)-(3.9) in time using package CVODE from SUNDIALS. The macroscopic rate coefficients are calculated using equation (3.36) and equation (3.37) at every time step for each group. This is required since the macroscopic group rate coefficients depend on the quadratic parameters which alter with time.

The comparison of the group properties is done for both 2 and 3 quadratic groups against the state-to-state simulation. The group properties from the state-to-state simulation are calculated in the post processing step since the output from the state-to-state simulation directly gives the population in each energy state at every time step. The population of each internal state is taken to compute the moments as well as the quadratic parameters. These are used to compare the results from the two models.

Figure 4.4 shows a comparison of the number of moles of each group for 2 and 3 groups. The solid lines represent the state-to-state results and the markers represent the quadratic model. It is observed that there is very good agreement between the two models for both 2 and 3 quadratic groups. The number of moles of group 1 decrease continuously in both cases. This is because there is no excitation to group 1 and internal excitation within the group does not change the number of moles within the group. The change in the number of moles in group 1 is due to excitation to higher energy groups and dissociation of the molecules into atoms. The initial constant value of the number of moles corresponds to the phase of the simulation when the energy transfer reactions within the group dominate. Hence the number of moles is not changing. This trend is in contrast to the evolution of the number of moles in other higher groups. The initial number of moles in the higher groups is very low. This is because at a temperature as low as 2,000 K most of the molecules are in the ground state or occupy the lowest energy states. As time evolves, the excitation reactions from the lower lying groups cause the mole fractions of the higher groups to increase and eventually reach a maximum. After the excitation processes become less prominent, dissociation reactions cause the number of moles to decrease and finally plateau at zero when all the nitrogen molecules have dissociated into nitrogen atoms.

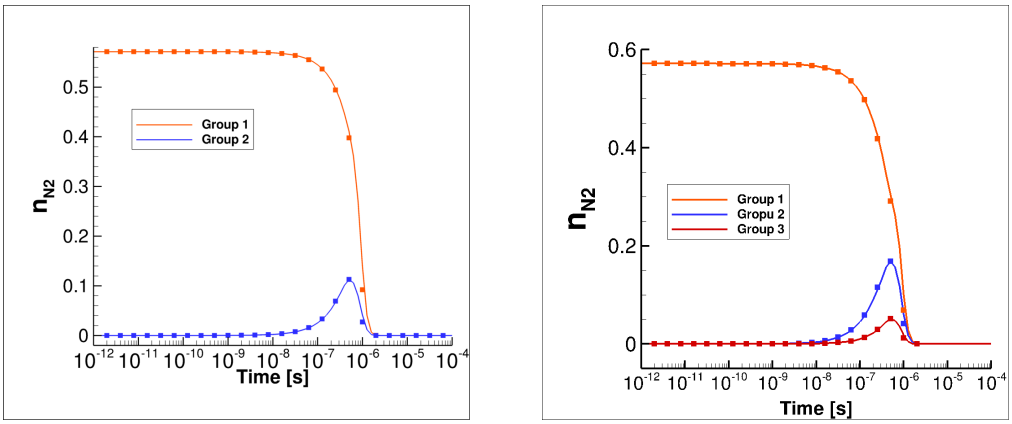

(a) 2 Bins (b) 3 Bins

Figure 4.4: Time evolution of number of moles in a group. The dots represent the quadratic model and the solid lines represent the full state-to-state model

First moment in the quadratic model corresponds to the internal energy within a group. The plot of the first moment of each group using the two models shows that the internal energy within each group first increases reaches a maximum and then decreases to finally become zero. The trend for all groups is the same since internal excitation within the group changes the internal energy within the group without changing the mole fraction. This is observed due to the fact that internal excitation within a group populates the higher energy states of the group. This increases the total internal energy of the group without changing its mole fraction. Finally, the decrease in the internal energies is due to the dissociation reactions gaining predominance over the energy transfer reactions.

Group 1 shows a higher internal energy at the start of the simulation because the lower energy states are most highly populated. Therefore, the rise in the internal energy also occurs first for group 1 since it is most highly populated and increasing the energy of the system by a small amount will excite energy states within group 1, populating the higher rovibrational levels within the group before excitation occurs to energy states belonging to the higher lying groups. This delay in the rise of internal energy is more observable while using 2 quadratic bins since the energy difference between the states lying in the 1^{st} and 2^{nd} groups is higher. Significant number of states belong to group 1 making internal excitation within the group predominant before excitation to higher group.

Unlike the behavior of the zeroth moment of the 1st group, the energy of this group reaches a supremum. This behavior is due to the fact that even though there is no change in the population present in group 1, excitation from the lower energy states to higher energy states belonging to that group increase the total energy of the group.

The group second moment plots show trends similar to internal energy plots. Figure 4.6 is a graph of the temporal evolution of the group second moment. In comparison to the full state-to-state model, the quadratic model shows good agreement with the state-of-the-art state-to-state modeling. Like the internal energy of the group, the group second moment for the state-to-state simulation is constructed from the population distribution solution. The group second moment, like the group internal energy first increases, reaches a maximum due to excitation dominance and then plummets to zero as dissociation takes precedence. Finally, the plot flattens at zero when all the molecules have dissociated.

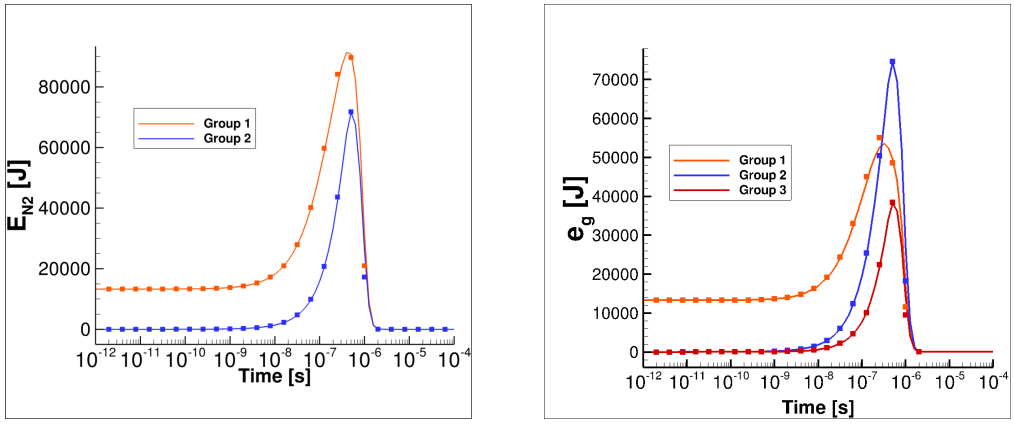

(a) 2 Bins (b) 3 Bins

Figure 4.5: Time evolution of Group internal energy

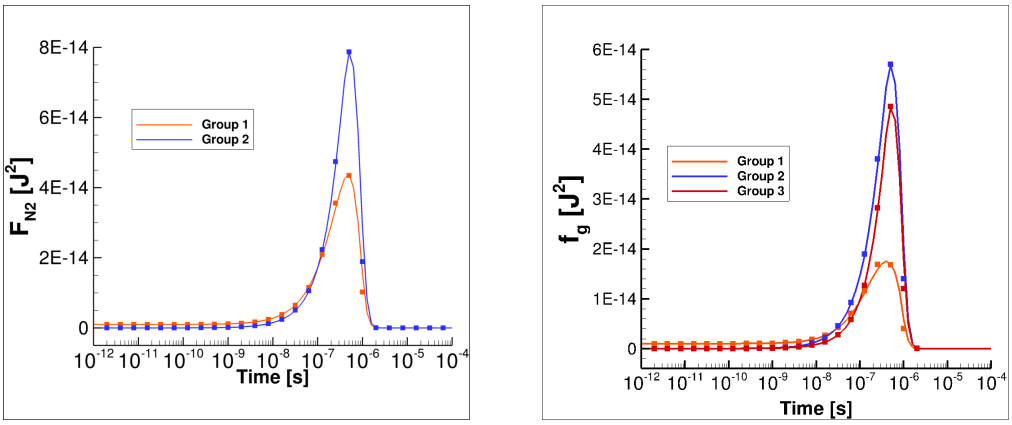

(a) 2 Bins (b) 3 Bins

Figure 4.6: Time evolution of Group second moment

Another important physical macroscopic quantity studied is the internal temperature of each group. The temperature for each group is computed using the energy state population distribution. To calculate the temperature, the following one dimensional non-linear equation is solved using KINSOL.

$$T = T(n_g, e_g) \tag{4.1}$$

Here, n_g and e_g are obtained by calculating the moments of the population distribution function for each group. The subscript 'g' corresponds to the group number. A linear reconstruction function is used to compute the moments of the distribution function where the linear term coefficient is inversely proportional to the internal temperature of the group. The equation given below shows the equation that is solved to find the group temperatures.

$$\frac{e_g}{n_g} = \frac{1}{Q_g} \sum_{i \epsilon I_g} g_i \ \varepsilon_i \ e^{-\varepsilon_i / k_B T}$$

The simulation starts at a temperature of 2,000 K and progresses to equilibrate at 20,000 K. A comparison of the temperatures obtained from the state-to-state and quadratic models at different time intervals show good agreement. All groups attain a final temperature of 20,000 K, the temperature of the reactor. In the case of 2 and 3 bins, a quasi-steady state is noticeable near the end of the simulation when the dissociation processes dominate.

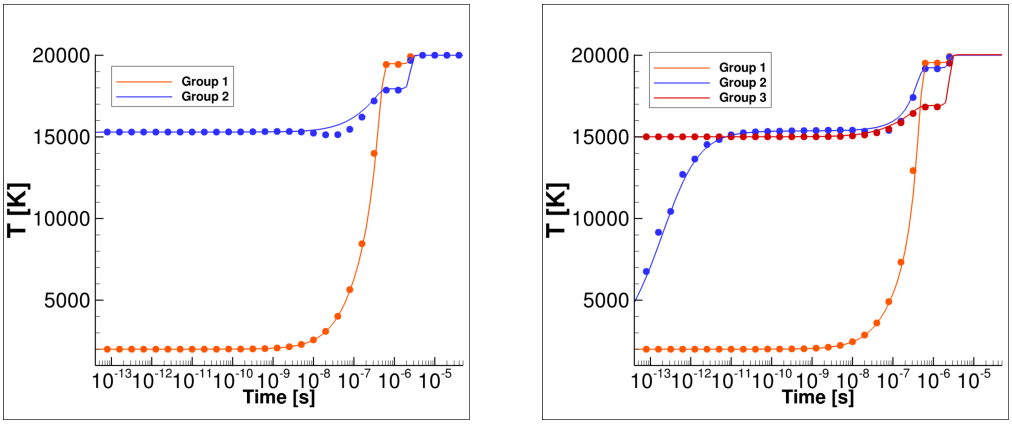

(a) 2 Bins (b) 3 Bins

Figure 4.7: Time evolution of Group Temperature

4.1.3 Comparison of the Global Values

This subsection comprises of comparisons of the global macroscopic properties of the molecule-atom system. The simulations are run for different number of groups: 1,2,3,5 and 7. In figure 4.8, global mole fractions of the nitrogen molecule are compared with the full state-to-state result. Grouping all the bound states in 1 group is not very efficient in representing the global properties. It deviates significantly from the full state model. As the number of groups is increased, the mole fraction values get closer to the state-to-state values. The zoomed in figure shows that the mole fraction values converge for groups 2,3,5 and 7. However, the difference in increasing the number of groups is justified by the better representation of the reconstructed population distribution as seen in section 4.1.1.

There are two phases of chemical reactions. Until around t= $3E-07$s there is minimal dissociation of the nitrogen molecule. The reactions occurring until this time are predominantly energy transfer(excitation and de-excitation) reactions. This first phase of transfer reaction dominance is followed by dissociation of nitrogen molecules. As the system evolves to the final state at 20,000K, in order to attain thermal equilibrium, the temperature of the system increases. The rate coefficients for dissociation are higher for higher temperatures. This means that the dissociation reactions will be faster at higher temperatures. Therefore, as the system temperature increases, the molecules are already excited and hence even slight increase in energy leads

to dissociation, making dissociation process more noticeable than the energy transfer processes. During dissociation, the mole fraction of the molecules decreases and evens out at zero after all the molecules are dissociated. The dissociation is complete and the system reaches chemical and thermal equilibrium by 3 μs.

In these high temperature regimes, it is noticed that the recombination rate coefficients are significantly smaller than the rate coefficients for the other kinetic processes and hence recombination processes have negligible effect on the mole fractions of various species present in the system.

The total internal energy as well as the total second moment of the nitrogen molecules show a similar progression. Figure 4.9a shows a comparison of the total internal energy of the molecules obtained from the state-to-state model and the quadratic model. It can be seen that the quadratic model is able to predict the first and second moment of the population distribution accurately.

The internal energy of the N_2 molecules is initially almost a constant since there are very few excitation and dissociation processes occurring at 2,000 K. As the system evolves, the high energy states become more populated due to excitation process, and the internal energy of the system increases. In this regime, the effect of the excitation processes on the internal energy are more dominant than the effect of the dissociation processes. Marching even further in time, the temperature of the system becomes high enough for the dissociation interactions to become predominant. This leads the internal energy of the system to decrease and finally plateau at zero when almost all the molecules are dissociated into atoms. The magnified view of the excitation and dissociation portion of the internal energy, figure 4.9b, shows that even with just 2 bins there is good convergence with the state-to-state model. Some deviation from the full simulation exists due to the type by binning strategy employed.

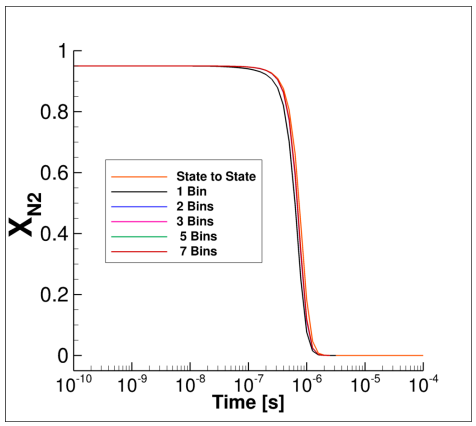

(a) Mole fraction of N_2 molecule

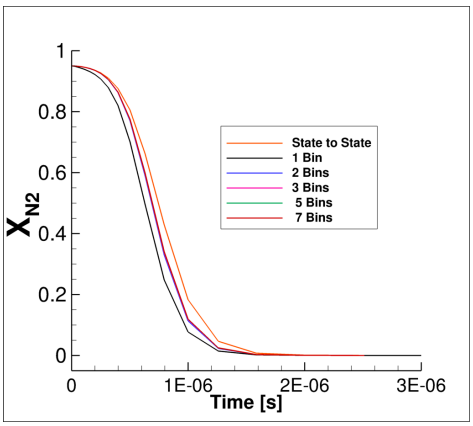

(b) Mole fraction profiles zoomed in during dissociation

Figure 4.8: Evolution of mole fractions in time

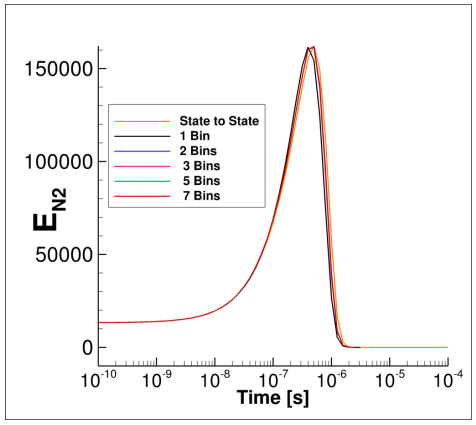

(a) Total internal energy of N_2 molecules

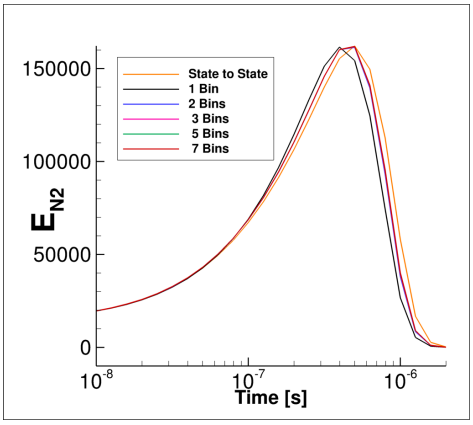

(b) Internal Energy zoomed in during dissociation

Figure 4.9: Evolution of the internal energy in time

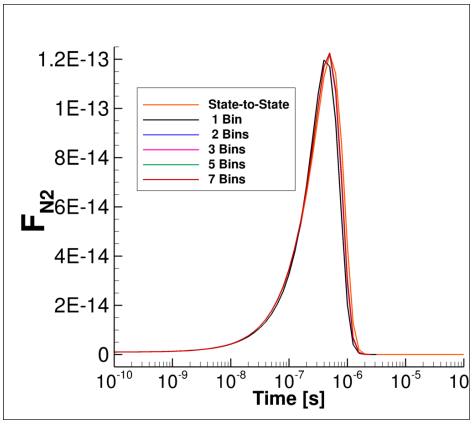

(a) Total second moment of the N_2 molecule

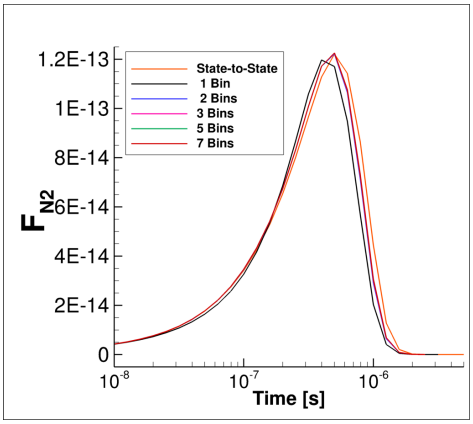

(b) Second moment zoomed in during dissociation

Figure 4.10: Evolution of the second moment in time

4.1.4 Comparison of Group Parameters

From the simulations, it is observed that the non-linear system of equations (3.34) is very stiff. The actual values of β and γ are of the order of the energy and energy square, the energy here corresponds to the rovibrational energy level of the molecule. The energies are of the order of a few electron volts. Hence to obtain more reasonable values of β and γ, the quadratic equation coefficients, the energy in the system is normalized with the value of the energy of the last bound level of the nitrogen molecule, 9.753 eV($\equiv \hat{\varepsilon}$). This energy corresponds to the dissociation limit of the nitrogen molecule. These new normalized parameters are distinguished by a hat. The normalized values of β and γ are related to the actual values by the following equations,

$$\hat{\beta} = \beta\hat{\varepsilon} \tag{4.2}$$

$$\hat{\gamma} = \gamma\hat{\varepsilon}^2 \tag{4.3}$$

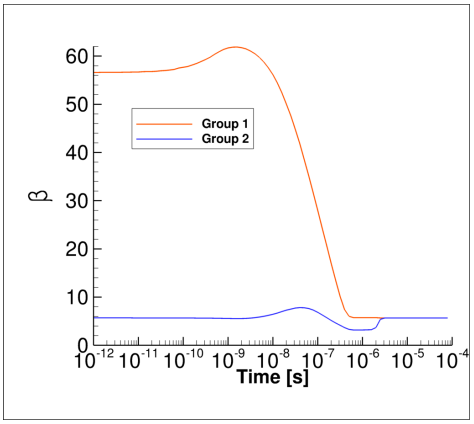

(a) Evolution of $\hat{\beta}$

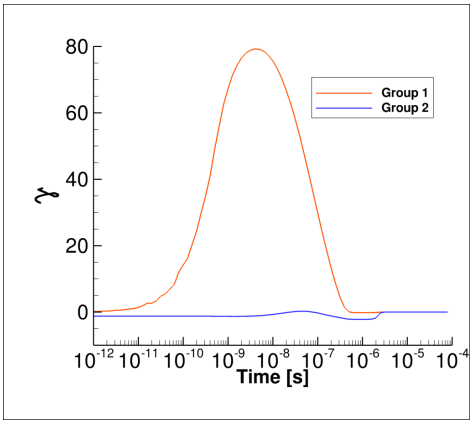

(b) Evolution of $\hat{\beta}$

Figure 4.11: Quadratic Parameters using 2 Groups

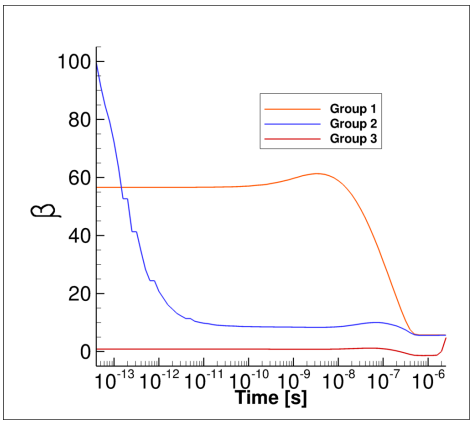

(a) Evolution of $\hat{\beta}$

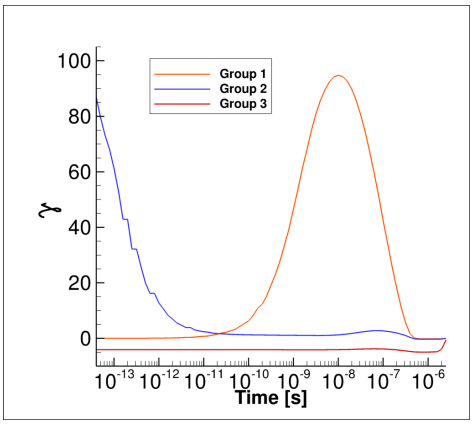

(b) Evolution of $\hat{\beta}$

Figure 4.12: Quadratic parameters using 3 Groups

From figures 4.11 and 4.12, it is seen that as the system approaches equilibrium, the slope and curvature values of all the groups start to converge. Further using equation (3.35) for the equilibrium condition, the temperatures of the groups are calculated and they are found to be very close to the final translational temperature of the system, 20,000 K. In equilibrium, the molecules attain a Boltzmann distribution and hence all higher order terms in the description of the population distribution become zero. The simulations of the quadratic model for the $N_2(^1\Sigma_g^+)$-$N(^4S_u)$ system also show similar trends. As the system approaches equilibrium, the $\hat{\gamma}$ values for all groups approach zero.

Figure 4.11a shows the evolution of $\hat{\beta}$ for each group in the 2 quadratic

group simulation. As soon as the simulation starts, group 2 slope value decreases almost instantly. The decreased value of the slope of group 2 corresponds closely to the slope value for the final temperature of 20,000 K. The slope of group 1 starts off with a value corresponding to the initial temperature of 2,000 K. Group 1 is initially in a frozen state and hence the slope and curvature value do not change. This is also observed in the population distribution plots. As time progresses, the slope of group 1 starts to decrease until the end when it attains the slope corresponding to the temperature of 20,000 K. Meanwhile, the curvature of group 1 increases. This can be observed from figure 4.11b. This increase in curvature corresponds to the strong non-equilibrium regime of the simulation. After reaching a maximum, the curvature of group 1 decreases and finally becomes zero when the system approaches and attains equilibrium. This is a requirement that the model is required to satisfy in order to give physically meaningful results. Group 2 curvature remains close to zero during most of the simulation. There is a slight deviation from the zero value during the time frame when the dissociation processes are dominant. This corresponds to the simulation time of 0.05 μs to 5 μs. After this time period, the curvature value goes to zero and the system attains equilibrium.

Figure 4.12 shows the progression of the quadratic parameters for 3 quadratic bins. Group 1 $\hat{\beta}$ value starts with a value corresponding to the Boltzmann distribution at 2,000 K, similar to the previous case of 2 quadratic groups. The trend can be distinguished in 3 regimes. The initial frozen regime, the dissociation regime and finally the equilibrium regime. The evolution of the normalized curvature value is similar to the progression observed in group 1 of 2 quadratic groups. Group 2 starts with an initial $\hat{\beta}$ higher than the group 1 value. The value then reduces continuously to attain a final value corresponding to the equilibrium distribution at 20,000 K. There are some steps observed in the figure for group 2. This is a numerical manifestation. The curvature parameter for group 2 also reduces continuously to attain a value of zero towards the end of the kinetic processes.

Group 3 shows a peculiar behavior. The slope parameter for group 3 starts off near zero at the beginning of the simulation. As time advances, the slope reduces to a negative value. This negative slope for group 3 should not be confused with a population inversion. This value of slope is just a parameter in the quadratic model which is combined with the curvature terms. These

two terms together define the nature of the population distribution in the levels belonging to this group. The anomalous behavior of the parameters of the 3^{rd} group is due to the high dissociation rate of the group. The curvature value also attains a negative value when dissociation reactions dominate the kinetics of the system.

The central portion with non-zero values for the group $\hat{\gamma}$ values is of interest whilst studying chemical non-equilibrium. As seen in section 4.1.1, the population distribution follows a non-Boltzmann distribution when there is chemical non-equilibrium. Hence, the representation of the population distribution needs to account for the curvature of the graph, which is accommodated by the maximum entropy quadratic model.

CHAPTER 5

CONCLUSION

This study is focused on advanced modeling of non-equilibrium flows for state-specific chemical kinetics based on a moment method combined with an energy state grouping strategy. A novel multi group maximum entropy model has been introduced in this thesis. This model comprises of a quadratic reconstruction operator to represent the population distribution function of the molecules in the energy space. Rovibrational non-equilibrium involving energy transfer and dissociation-recombination reactions of the $N_2(^1\Sigma_g^+)$-$N(^4S_u)$ system are studied. The kinetic and thermodynamic data is obtained from *ab initio* calculations performed at NASA Ames Research Center. 7421 bound levels of the nitrogen molecule are lumped together in groups based on the energy of the quantum mechanical states (energy based grouping strategy). The macroscopic governing equations are formulated based on the method of moments. The macroscopic master equations are solved to obtain the group moment value which are used to reconstruct the population distribution in the energy space; the quadratic parameters are calculated from the group properties/moments. The population distribution function within each group is subject to constraints. These constraints are the moment conservation equations. In the quadratic model, the first three moments of the distribution function are chosen. Therefore, there are three constraints on the equation. This makes the problem over-constrained. To solve this over-constrained system the method of Lagrange multipliers is used to obtain a solution. The Lagrange multipliers correspond to the coefficients of the reconstruction polynomial.

The macroscopic equations are derived from the exact microscopic governing equations by taking its moments and summing up the levels belonging to a particular group. This reduces the order of the ordinary differential equations to be solved. The group rate coefficients, which characterize the kinetics amongst groups, are computed directly from the microscopic rates which are

obtained from first principles. Therefore, in the computation of group properties no ad hoc assumptions are made and hence this model retains most of the physics of the system.

To study and validate the quadratic model, various test cases with different number of groups are simulated and compared with the state-of-the-art state-to-state model. To emphasize the advantage of a quadratic reconstruction function, simulations are compared against a linear reconstruction function as well. From the state-to-state simulations, it is observed that the intermediate non-equilibrium regime between the initial and final equilibrium population distribution has an inherent curvature associated with the distribution function. Using a linear type of reconstruction forces the states belonging to a group to be in equilibrium at a particular group temperature. Hence, the linear model is not suitable for depicting the curvature of the distribution function. In order to capture the distribution function with reasonable accuracy, it will be imperative to use a large number of groups. This drawback in the linear model is overcome by introducing a quadratic term in the reconstruction polynomial, making it a second order polynomial. With the inclusion of the quadratic term, the number of groups required to represent the population distribution function reduces significantly.

A comparison of the population distribution function using the three models shows that the quadratic model captures the non-Boltzmann distribution functions with good accuracy with just two and three groups. A comparison of the group properties and global properties show good agreement between the quadratic and the state-to-state model. The internal temperature profiles obtained from the two models match and the group temperatures finally reach the temperature of 20,000 K which is the temperature of the reactor. Since at equilibrium, the distribution function becomes the Boltzmann distribution at the equilibrium temperature, this implies that the curvature of the distribution plot goes to zero and the slope of the plot becomes inversely proportional to the temperature of the system. Studying the time evolution of the quadratic function parameters, the trends show that the curvature term, γ_g goes to zero for all groups when the system reaches the final equilibrium state and the value of β_g attains a value corresponding to the final equilibrium temperature. This shows that the quadratic model is able to represent the final equilibrium state of the system correctly which is an important condition to be satisfied by the model.

The key contribution of the multi group maximum entropy quadratic model is the introduction of the curvature parameter in the reconstruction function. It is able to accurately capture the behavior of the population density in the entire span of the phase space at all times. Using the maximum entropy quadratic model results in a reduction of the number of groups required to represent the energy space of the molecule, thereby leading to a reduction of the computational time required to simulate the non-equilibrium processes while still maintaining good accuracy.

In future, this chemistry model will be coupled with the flow equations introducing new energy conservation equations corresponding to the number of groups used and second moment conservation equations. There will also be more continuity equations introduced which will also depend on the number of groups in the molecule system. The following equations represent the flow equations with the chemistry model developed in this thesis.

$$\frac{\partial \rho^g}{\partial t} + \nabla.(\rho^g u \ + J^g) = \dot{\omega^g} \tag{5.1}$$

$$\frac{\partial e^g}{\partial t} + \nabla.(\rho^g u e^g \ + J^g e^g) = \dot{\Omega_e^g} \tag{5.2}$$

$$\frac{\partial f^g}{\partial t} + \nabla.(\rho^g u f^g \ + J^g f^g) = \dot{\Omega_f^g} \tag{5.3}$$

Here, $\dot{\omega^g}$, $\dot{\Omega_e^g}$ and $\dot{\Omega_f^g}$ represent the chemical source terms obtained from equations (3.7) - (3.9).

APPENDIX A

MACROSCOPIC GROUP RATES

The macroscopic group rates can be derived as follows.

A.1 Macroscopic group rate for population density

$$\sum_{i\epsilon I_g}\frac{dn^i_{N_2}}{dt}=\sum_{h\epsilon n}\sum_{i\epsilon I_g}\sum_{j\epsilon I_h}\left[-k_{i,j}n^i_{N_2}n_N\,\frac{n^g_{N_2}}{n^g_{N_2}}+k_{j,i}n^j_{N_2}n_N\,\frac{n^h_{N_2}}{n^h_{N_2}}\right]+\sum_{i\epsilon I_g}\left[-k^d_i n^i_{N_2}n_N\frac{n^g_{N_2}}{n^g_{N_2}}+k^r_i n^3_N\right]$$

$$\begin{aligned}
{}^0K_{g,h} &= \sum_{i\epsilon I_g}\sum_{j\epsilon I_h}\frac{k_{i,j}n^i_{N_2}}{n^g_{N_2}}\\
&= \sum_{i\epsilon I_g}\sum_{j\epsilon I_h}\frac{k_{i,j}g_i e^{-\alpha_g-\beta_g\varepsilon_i-\gamma_g\varepsilon_i^2}}{n^g_{N_2}}\\
&= \sum_{i\epsilon I_g}\sum_{j\epsilon I_h}\frac{k_{i,j}g_i n^g_{N_2}e^{-\beta_g\varepsilon_i-\gamma_g\varepsilon_i^2}}{Q_g n^g_{N_2}}\\
&= \frac{1}{Q_g}\sum_{i\epsilon I_g}\sum_{j\epsilon I_h}k_{i,j}g_i e^{-\beta_g\varepsilon_i-\gamma_g\varepsilon_i^2} \qquad \text{(A.1)}
\end{aligned}$$

$$\begin{aligned}
{}^0C^d_g &= \sum_{i\epsilon I_g}\frac{k^d_i n^i_{N_2}}{n^g_{N_2}}\\
&= \sum_{i\epsilon I_g}\frac{k^d_i g_i e^{-\alpha_g-\beta_g\varepsilon_i-\gamma_g\varepsilon_i^2}}{n^g_{N_2}}\\
&= \sum_{i\epsilon I_g}\frac{k^d_i g_i n^g_{N_2}e^{-\beta_g\varepsilon_i-\gamma_g\varepsilon_i^2}}{Q_g n^g_{N_2}}\\
&= \frac{1}{Q_g}\sum_{i\epsilon I_g}k^d_i g_i e^{-\beta_g\varepsilon_i-\gamma_g\varepsilon_i^2} \qquad \text{(A.2)}
\end{aligned}$$

$$ {}^{0}C_g^r = \sum_{i \epsilon I_g} k_i^r \tag{A.3} $$

Where,

$$ Q_g = \sum_{i \epsilon I_g} g_i e^{-\beta_g \varepsilon_i - \gamma_g \varepsilon_i^2} \tag{A.4} $$

A.2 Macroscopic group rate for internal energy density

$$ \begin{aligned} \sum_{i \epsilon I_g} \frac{de_{N_2}^i}{dt} &= \sum_{h \epsilon n} \sum_{i \epsilon I_g} \sum_{j \epsilon I_h} \left[-k_{i,j}^e \varepsilon_i n_{N_2}^i n_N \frac{e_{N_2}^g}{e_{N_2}^g} + k_{j,i}^e \varepsilon_i n_{N_2}^j n_N \frac{e_{N_2}^h}{e_{N_2}^h} \right] \\ &+ \sum_{i \epsilon I_g} \left[-k_i^d \varepsilon_i n_{N_2}^i n_N \frac{e_{N_2}^g}{e_{N_2}^g} + k_i^r \varepsilon_i n_N^3 \right] \end{aligned} \tag{A.5} $$

$$ \begin{aligned} {}^{1}K_{g,h} &= \sum_{i \epsilon I_g} \sum_{j \epsilon I_h} \frac{k_{i,j} \varepsilon_i n_{N_2}^i}{e_{N_2}^g} \\ &= \frac{\sum_{i \epsilon I_g} \sum_{j \epsilon I_h} k_{i,j} \varepsilon_i g_i e^{-\alpha_g - \beta_g \varepsilon_i - \gamma_g \varepsilon_i^2}}{\sum_{i \epsilon I_g} n_{N_2}^i \varepsilon_i} \\ &= \frac{\sum_{i \epsilon I_g} \sum_{j \epsilon I_h} k_{i,j} \varepsilon_i g_i \frac{n_{N_2}^g}{Q_g} e^{-\beta_g \varepsilon_i - \gamma_g \varepsilon_i^2}}{\sum_{i \epsilon I_g} \varepsilon_i g_i \frac{n_{N_2}^g}{Q_g} e^{-\beta_g \varepsilon_i - \gamma_g \varepsilon_i^2}} \\ &= \frac{1}{Q_g^e} \sum_{i \epsilon I_g} \sum_{j \epsilon I_h} k_{i,j} \varepsilon_i g_i e^{-\beta_g \varepsilon_i - \gamma_g \varepsilon_i^2} \end{aligned} \tag{A.6} $$

$$
\begin{aligned}
{}^1C_g^d &= \sum_{i\epsilon I_g} \frac{k_i^d \varepsilon_i n_{N_2}^i}{e_{N_2}^g} \\
&= \frac{\sum\limits_{i\epsilon I_g} k_i^d \varepsilon_i g_i e^{-\alpha_g - \beta_g \varepsilon_i - \gamma_g \varepsilon_i^2}}{\sum\limits_{i\epsilon I_g} n_{N_2}^i \varepsilon_i} \\
&= \frac{\sum\limits_{i\epsilon I_g} k_i^d \varepsilon_i g_i e^{-\alpha_g - \beta_g \varepsilon_i - \gamma_g \varepsilon_i^2}}{\sum\limits_{i\epsilon I_g} \varepsilon_i g_i e^{-\alpha_g - \beta_g \varepsilon_i - \gamma_g \varepsilon_i^2}} \\
&= \frac{1}{Q_g^e} \sum_{i\epsilon I_g} k_i^d \varepsilon_i g_i e^{-\beta_g \varepsilon_i - \gamma_g \varepsilon_i^2} \qquad \text{(A.7)}
\end{aligned}
$$

$$
{}^1C_g^r = \sum_{i\epsilon I_g} k_i^r \varepsilon_i \qquad \text{(A.8)}
$$

Where,

$$
Q_g^e = \sum_{i\epsilon I_g} \varepsilon_i g_i e^{-\beta_g \varepsilon_i - \gamma_g \varepsilon_i^2} \qquad \text{(A.9)}
$$

A.3 Macroscopic group rate for the function '$n_i \varepsilon_i^2$'

$$
\begin{aligned}
\sum_{i\epsilon I_g} \frac{df_{N_2}^i}{dt} &= \sum_{h\epsilon n} \sum_{i\epsilon I_g} \sum_{j\epsilon I_h} \left[-k_{i,j} \varepsilon_i^2 n_{N_2}^i n_N \frac{f_{N_2}^g}{f_{N_2}^g} + k_{j,i} \varepsilon_i^2 n_{N_2}^j n_N \frac{f_{N_2}^h}{f_{N_2}^h} \right] \qquad \text{(A.10)} \\
&+ \sum_{i\epsilon I_g} \left[-k_i^d \varepsilon_i^2 n_{N_2}^i n_N \frac{f_{N_2}^g}{f_{N_2}^g} + k_i^r \varepsilon_i^2 n_N^3 \right]
\end{aligned}
$$

$$
\begin{aligned}
{}^2K_{g,h} &= \sum_{i\epsilon I_g}\sum_{j\epsilon I_h}\frac{k_{i,j}\varepsilon_i^2 n^i_{N_2}}{f^g_{N_2}} \\
&= \frac{\sum\limits_{i\epsilon I_g}\sum\limits_{j\epsilon I_h} k_{i,j}\varepsilon_i^2 g_i e^{-\alpha_g-\beta_g\varepsilon_i-\gamma_g\varepsilon_i^2}}{\sum\limits_{i\epsilon I_g} n^i_{N_2}\varepsilon_i^2} \\
&= \frac{\sum\limits_{i\epsilon I_g}\sum\limits_{j\epsilon I_h} k_{i,j}\varepsilon_i^2 g_i \frac{n^g_{N_2}}{Q_g} e^{-\beta_g\varepsilon_i-\gamma_g\varepsilon_i^2}}{\sum\limits_{i\epsilon I_g}\varepsilon_i^2 g_i \frac{n^g_{N_2}}{Q_g} e^{-\beta_g\varepsilon_i-\gamma_g\varepsilon_i^2}} \\
&= \frac{1}{Q^f_g}\sum_{i\epsilon I_g}\sum_{j\epsilon I_h} k_{i,j}\varepsilon_i^2 g_i e^{-\beta_g\varepsilon_i-\gamma_g\varepsilon_i^2} \qquad \text{(A.11)}
\end{aligned}
$$

$$
\begin{aligned}
{}^2C^d_g &= \sum_{i\epsilon I_g}\frac{k^d_i\varepsilon_i^2 n^i_{N_2}}{f^g_{N_2}} \\
&= \frac{\sum\limits_{i\epsilon I_g} k^d_i\varepsilon_i^2 g_i e^{-\alpha_g-\beta_g\varepsilon_i-\gamma_g\varepsilon_i^2}}{\sum\limits_{i\epsilon I_g} n^i_{N_2}\varepsilon_i^2} \\
&= \frac{\sum\limits_{i\epsilon I_g} k^d_i\varepsilon_i^2 g_i e^{-\alpha_g-\beta_g\varepsilon_i-\gamma_g\varepsilon_i^2}}{\sum\limits_{i\epsilon I_g}\varepsilon_i^2 g_i e^{-\alpha_g-\beta_g\varepsilon_i-\gamma_g\varepsilon_i^2}} \\
&= \frac{1}{Q^f_g}\sum_{i\epsilon I_g} k^d_i\varepsilon_i^2 g_i e^{-\beta_g\varepsilon_i-\gamma_g\varepsilon_i^2} \qquad \text{(A.12)}
\end{aligned}
$$

$$
{}^2C^r_g = \sum_{i\epsilon I_g} k^r_i\varepsilon_i^2 \qquad \text{(A.13)}
$$

Where,

$$
Q^f_g = \sum_{i\epsilon g}\varepsilon_i^2 g_i e^{-\beta_g\varepsilon_i-\gamma_g\varepsilon_i^2} \qquad \text{(A.14)}
$$

REFERENCES

[1] David W Schwenke. Dissociation cross sections and rates for nitrogen. Technical report, DTIC Document, 2009.

[2] Galina Chaban, Richard Jaffe, David W Schwenke, and Winifred Huo. Dissociation cross sections and rate coefficients for nitrogen from accurate theoretical calculations. *AIAA paper*, 1209:2008, 2008.

[3] Richard Jaffe, David Schwenke, Galina Chaban, and Winifred Huo. Vibrational and rotational excitation and relaxation of nitrogen from accurate theoretical calculations. In *46th AIAA Aerospace Sciences Meeting and Exhibit*, page 1208, 2008.

[4] Richard Jaffe, David Schwenke, and Galina Chaban. Theoretical analysis of n2 collisional dissociation and rotation-vibration energy transfer. *AIAA paper*, 1569:2009, 2009.

[5] Richard Jaffe, David Schwenke, and Galina Chaban. Vibrational and rotational excitation and dissociation in n2-n2 collisions from accurate theoretical calculations. *AIAA Paper*, 4517:2010, 2010.

[6] John ZH Zhang and William H Miller. Quantum reactive scattering via the s-matrix version of the kohn variational principle: Integral cross sections for h+ h 2 (ν 1= j 1= 0) h 2 (ν 2= 1, j 2= 1, 3)+ h in the energy range e total= 0.9–1.4 ev. *Chemical physics letters*, 153(6):465–470, 1988.

[7] David W Schwenke. Calculations of rate constants for the three-body recombination of h2 in the presence of h2. *The Journal of chemical physics*, 89(4):2076–2091, 1988.

[8] F Esposito, M Capitelli, and C Gorse. Quasi-classical dynamics and vibrational kinetics of n+ n 2 (v) system. *Chemical Physics*, 257(2): 193–202, 2000.

[9] Dunyou Wang, James R Stallcop, Winifred M Huo, Christopher E Dateo, David W Schwenke, Harry Partridge, and Dochan Kwak. Quantal study of the exchange reaction for n+ n2 using an ab initio potential energy surface. 2002.

[10] Chul Park. Assessment of a two-temperature kinetic model for dissociating and weakly ionizing nitrogen. *Journal of Thermophysics and Heat Transfer*, 2(1):8–16, 1988.

[11] A Aliat, A Chikhaoui, and EV Kustova. Nonequilibrium kinetics of a radiative co flow behind a shock wave. *Physical Review E*, 68(5):056306, 2003.

[12] Marco Panesi, Thierry Magin, Anne Bourdon, Arnaud Bultel, and Olivier Chazot. Fire ii flight experiment analysis by means of a collisional-radiative model. *Journal of Thermophysics and Heat Transfer*, 23(2):236–248, 2009.

[13] M Panesi, TE Magin, A Munafò, A Bourdon, R Jaffe, and DW Schwenke. Rovibrational internal energy excitation and dissociation of nitrogen in hypersonic flows. In *Proceedings of the Summer Program*, page 445. Citeseer, 2010.

[14] Marco Panesi, TE Magin, Anne Bourdon, Arnaud Bultel, and Olivier Chazot. Electronic excitation of atoms and molecules for the fire ii flight experiment. *Journal of Thermophysics and Heat Transfer*, 25(3): 361–374, 2011.

[15] Thierry E Magin, Marco Panesi, Anne Bourdon, Richard L Jaffe, and David W Schwenke. Coarse-grain model for internal energy excitation and dissociation of molecular nitrogen. *Chemical Physics*, 398:90–95, 2012.

[16] A Munafò, M Panesi, and TE Magin. Boltzmann rovibrational collisional coarse-grained model for internal energy excitation and dissociation in hypersonic flows. *Physical Review E*, 89(2):023001, 2014.

[17] A Munafò and TE Magin. Modeling of stagnation-line nonequilibrium flows by means of quantum based collisional models. *Physics of Fluids (1994-present)*, 26(9):097102, 2014.

[18] Yen Liu, Marcel Vinokur, Marco Panesi, and Thierry Magin. A multigroup maximum entropy model for thermo-chemical nonequilibrium. *AIAA paper*, 4332:2010, 2010.

[19] Yen Liu, Marco Panesi, Marcel Vinokur, and Peter Clarke. Microscopic simulation and macroscopic modeling of thermal and chemical non-equilibrium gases. *AIAA paper*, 3146:2013, 2013.

[20] Yen Liu, Marco Panesi, Amal Sahai, and Marcel Vinokur. General multi-group macroscopic modeling for thermo-chemical non-equilibrium gas mixtures. *The Journal of chemical physics*, 142(13):134109, 2015.

[21] Alessandro Munafo, Simone Venturi, Robyn Macdonald, and Marco Panesi. State-to-state and reduced-order models for dissociation and energy transfer in aerothermal environments.

[22] M Panesi, A Munafò, TE Magin, and RL Jaffe. Nonequilibrium shock-heated nitrogen flows using a rovibrational state-to-state method. *Physical Review E*, 90(1):013009, 2014.

[23] A Munafò, Y Liu, and M Panesi. Physical models for dissociation and energy transfer in shock-heated nitrogen flows. *Phys. Fluids*, 27(12): 127101, 2015.

[24] Aurélien Guy, Anne Bourdon, and Marie-Yvonne Perrin. Consistent multi-internal-temperatures models for nonequilibrium nozzle flows. *Chemical Physics*, 420:15–24, 2013.

[25] G Colonna, M Tuttafesta, M Capitelli, and D Giordano. Non-arrhenius no formation rate in one-dimensional nozzle airflow. *Journal of thermophysics and heat transfer*, 13(3):372–375, 1999.

[26] G Colonna and M Capitelli. Self-consistent model of chemical, vibrational, electron kinetics in nozzle expansion. *Journal of thermophysics and heat transfer*, 15(3):308–316, 2001.

[27] Alessandro Munafo, Marco Panesi, RL Jaffe, Gianpiero Colonna, Anne Bourdon, and TE Magin. Qct-based vibrational collisional models applied to nonequilibrium nozzle flows. *The European Physical Journal D*, 66(7):1–11, 2012.

[28] A Munafò, A Lani, A Bultel, and M Panesi. Modeling of non-equilibrium phenomena in expanding flows by means of a collisional-radiative model. *Physics of Plasmas (1994-present)*, 20(7):073501, 2013.

[29] A Munafò, SA Alfuhaid, J-L Cambier, and M Panesi. A tightly coupled non-equilibrium model for inductively coupled radio-frequency plasmas. *Journal of Applied Physics*, 118(13):133303, 2015.

[30] Jean-Luc Cambier and Stephane Moreau. Simulations of a molecular plasma in collisional-radiative nonequilibrium. In *AIAA, 24th Plasmadynamics and Lasers Conference*, volume 1, 1993.

[31] Arnaud Bultel, Bruno G Cheron, Anne Bourdon, Ousmanou Motapon, and Ioan F Schneider. Collisional-radiative model in air for earth reentry problems. *Physics of plasmas*, 13(4):43502–43502, 2006.

[32] M Capitelli, I Armenise, D Bruno, M Cacciatore, R Celiberto, G Colonna, O De Pascale, P Diomede, F Esposito, C Gorse, et al. Non-equilibrium plasma kinetics: a state-to-state approach. *Plasma Sources Science and Technology*, 16(1):S30, 2007.

[33] Fabrizio Esposito, Iole Armenise, and Mario Capitelli. N–n 2 state to state vibrational-relaxation and dissociation rates based on quasiclassical calculations. *Chemical Physics*, 331(1):1–8, 2006.

[34] F Esposito and M Capitelli. Quasiclassical molecular dynamic calculations of vibrationally and rotationally state selected dissociation cross-sections: N+ n 2 (v, j) 3n. *Chemical physics letters*, 302(1):49–54, 1999.

[35] Eswar Josyula, William F Bailey, and Stephen M Ruffin. Reactive and nonreactive vibrational energy exchanges in nonequilibrium hypersonic flows. *Physics of Fluids (1994-present)*, 15(10):3223–3235, 2003.

[36] Marco Panesi and Andrea Lani. Collisional radiative coarse-grain model for ionization in air. *Physics of Fluids (1994-present)*, 25(5):057101, 2013.

[37] MG Kapper and J-L Cambier. Ionizing shocks in argon. part i: Collisional-radiative model and steady-state structure. *Journal of applied physics*, 109(11):113308, 2011.

[38] MG Kapper and J-L Cambier. Ionizing shocks in argon. part ii: Transient and multi-dimensional effects. *Journal of Applied Physics*, 109(11): 113309, 2011.

[39] Alessandro Munafo, Michael G Kapper, Jean-Luc Cambier, and Thierry E Magin. Investigation of nonequilibrium effects in axisymmetric nozzle and blunt body nitrogen flows by means of a reduced rovibrational collisional model. *AIAA paper*, 647:135, 2012.

[40] Chul Park. Assessment of two-temperature kinetic model for ionizing air. *Journal of Thermophysics and Heat Transfer*, 3(3):233–244, 1989.

[41] Chul Park. Review of chemical-kinetic problems of future nasa missions. i-earth entries. *Journal of Thermophysics and Heat transfer*, 7(3):385–398, 1993.

[42] Chul Park, Richard L Jaffe, and Harry Partridge. Chemical-kinetic parameters of hyperbolic earth entry. *Journal of Thermophysics and Heat transfer*, 15(1):76–90, 2001.

[43] Harold Grad. On the kinetic theory of rarefied gases. *Communications on pure and applied mathematics*, 2(4):331–407, 1949.

[44] C David Levermore. Moment closure hierarchies for kinetic theories. *Journal of statistical Physics*, 83(5-6):1021–1065, 1996.

[45] Sydney Chapman and Thomas George Cowling. *The mathematical theory of non-uniform gases: an account of the kinetic theory of viscosity, thermal conduction and diffusion in gases*. Cambridge university press, 1970.

[46] L Landau and E Teller. Theory of sound dispersion. *Physikalische zeitschrift der Sowjetunion*, 10(34):34–43, 1936.

[47] Amal Sahai, Bruno E Lopez, Christopher O Johnston, and Marco Panesi. A reduced order maximum entropy model for chemical and thermal non-equilibrium in high temperature co2 gas. In *46th AIAA Thermophysics Conference*, page 3695, 2016.

[48] Amal Sahai, Bruno E Lopez, Christopher O Johnston, and Marco Panesi. Novel approach for co2 state-to-state modeling and application to multidimensional entry flows. In *55th AIAA Aerospace Sciences Meeting*, page 0213, 2017.

[49] Robyn Macdonald, Alessandro Munafo, and Marco Panesi. Rovibrational grouping for n_2 ($^1\sigma_g^+$) - n_2 ($^1\sigma_g^+$) energy transfer using state-to-state model. *AIAA Paper*, 2016.

[50] Herbert B Callen. *Thermodynamics & an Intro. to Thermostatistics*. John wiley & sons, 2006.

[51] KO Bowman and LR Shenton. Estimation: Method of moments. *Encyclopedia of statistical sciences*, 2004.

[52] Joakim Munkhammar, Lars Mattsson, and Jesper Rydén. Polynomial probability distribution estimation using the method of moments. *PloS one*, 12(4):e0174573, 2017.

[53] Alan C Hindmarsh, Peter N Brown, Keith E Grant, Steven L Lee, Radu Serban, Dan E Shumaker, and Carol S Woodward. Sundials: Suite of nonlinear and differential/algebraic equation solvers. *ACM Transactions on Mathematical Software (TOMS)*, 31(3):363–396, 2005.